Hydraulic Consequences of Invasive *Hydrilla* (submerged aquatic vegetation) in Tidal Channels: Implications for Wetland Maintenance

Brittany Jenner
GEOL394H
Advisor: Dr. Karen Prestegaard
April 30, 2010

Table of Contents

List of Figures

List of Tables

Abstract

Tidal marshes maintain elevation during periods of sea-level rise by the accumulation of both mineral sediment and organic matter. Sediment that is deposited on marsh surfaces must first be transported up tidal channel networks. Channel hydraulic characteristics exert significant controls on the sediment flux into marsh systems. The purpose of this study is to evaluate the effect of submerged aquatic vegetation on tidal channel discharge, velocity, and suspended transport potential by measurement and analysis of tidal channel shear velocity, vegetative roughness height, and hydraulic geometry. Field measurements were made in a freshwater wetland along the Patuxent River in Anne Arundel County, Maryland. Measurements were made in late summer-early fall when *Hydrilla* (an invasive species in the Chesapeake region) was at maximum height and density. The data indicate that the effective cross sectional area of flow is significantly reduced by vegetation. The tidal channels have high values of flow resistance and low values of velocity when compared with measurements from other similar tidal networks. Field measurements indicate that vegetative flow resistance is its maximum when flow depths are near their maximum; this significantly reduces the maximum flux of water in the tidal network. The network hydraulic geometry indicates that channel velocity for "bankfull" conditions decreases significantly in the upstream marsh channels, which is different from other tidal networks and the theoretical conditions for marsh systems. This upmarsh decrease in channel velocity affects the transport distance of water and sediment into the marsh. During summer months, the high tide does not convey water and sediment from the network mouth to the upstream tidal channels and marsh surfaces.

Table of Symbols

Symbol	Description
A	cross sectional area
a	width coefficient in hydraulic geometry power relationship
$(aC_D)^{-1}$	thickness of the deflected vegetation
b	hydraulic geometry exponent for width
c	depth coefficient in hydraulic geometry power relationship
C_D	drag coefficient
$C_D^{'}$	vegetal drag coefficient
d	mean channel depth; H = d
f	hydraulic geometry exponent for depth
g	acceleration due to gravity
H	mean channel depth
h	height of vegetation; h = Zo
κ	Von Karman's constant
K	conductance coefficient
k	velocity coefficient in hydraulic geometry power relationship
m	hydraulic geometry exponent for velocity
n	Manning's roughness coefficient
p	depth exponent in general power-law hydraulic equation
Q	discharge
q	slope exponent in general power-law hydraulic equation
r	channel shape
ř	channel shape estimator
S	water surface gradient
u	local velocity
U	maximum velocity
$\bar{u}$	mean velocity
u^*	shear velocity
u*´	vegetative shear velocity
w	mean surface width
W^*	bankfull width
x	horizontal distance from the center of the channel
y	distance upstream
Y_m^*	maximum bankfull depth
Z	relative height
Z^*	height of the channel bed above the lowest channel elevation
z	hydraulic geometry exponent for slope
Zm	height of plane of momentum absorption
Zo	height above bed where velocity is zero
λ	vegetal area fraction per unit length of channel

Introduction

1.1 Response of tidal marshes to sea level rise

Tidal marshes experience hydrologic changes on daily, seasonal, and longer time scales (Hughes et al., 1998). Marsh surfaces are exposed at low tide and are covered by water at high tide (Morris et al., 2002). Tidal magnitude varies throughout a lunar month. Tidal rivers that directly connect to terrestrial rivers also experience seasonal variations in streamflow that are overprinted by tidal changes (Morse et al., 2004). Sea level rise is a long-term change that affects tidal wetlands (Morris et al., 2002; Rybczyk and Cahoon, 2002). A wetland that maintains marsh surface elevation is considered to be in equilibrium. Four main factors that affect wetland equilibrium are: accretion, subsidence, sea level rise and sediment supply (Kirwan and Murray, 2007; Morris et al., 2002; Rybczyk and Cahoon, 2002; Wang et al., 1993). Accretion is the accumulation of sediment and organic matter in a wetland. Sediment supply, vegetation patterns and organic matter production affect marsh accretion rates (Morris et al., 2002; Rybczyk and Cahoon, 2002). Subsidence occurs as sediments compact; there can be both local and regional compaction terms (Rybczyk and Cahoon, 2002). Subsidence lowers the elevation of the marsh surface with respect to sea level. Tidal marshes that maintain their form as sea level rises must balance subsidence and sea level rise rates with vertical accretion rates of organic matter and mineral sediments.

Recent studies provide insight into the complex factors that affect organic and sediment accumulation necessary to maintain marsh equilibrium as sea level rises (e.g. Kirwan and Murray, 2007; Morris et al., 2002; Nyman and DeLaune, 1999; Rybczyk and Cahoon, 2002; and Turner et al., 2009). Kirwan and Murray (2007) developed a 3D model to examine marsh accretion, network development, sediment transport and biomass productivity. They modeled the effect of sea level rise on vegetated and non-vegetated wetlands and suggested that organic matter accumulation (vegetation) is required to maintain wetlands under scenarios with increasing sea level rise rates (Kirwan and Murray, 2007). Rybczyk and Cahoon (2002) used multiple models to study two salt marshes in coastal Louisiana, a region with high regional subsidence rates. Using field data on accumulation rates and a variety of sea level rise and subsidence scenarios, they concluded that both marshes would not be able to maintain elevation unless pulses of sediment-laden water (e.g. Mississippi River water) flooded the marshes. One might consider that nutrient loading of coastal environments would lead to higher rates of organic matter accretion. Turner et al. (2009) sampled ten different salt marsh plots that had been given specific dosages of nitrogen and phosphorus during growing seasons since the 1970s. They analyzed organic and inorganic content and marsh elevation. They concluded that eutrophication did not increase marsh soil accretion. In fact, nutrient loading decreases biomass accumulation at depth and has little affect on shallow biomass and inorganic sediment accumulation (Turner et al., 2009).

These previous studies suggest that organic matter accumulation alone is not sufficient to maintain marshes in sea level rise scenarios, particularly in eutrophic environments. Therefore, in this study I focus on hydraulic controls on sediment transport into complex tidal network marsh systems. Freshwater tidal marshes are found at the upstream end of tidal estuaries and are usually near supplies of sediment that can help maintain the marshes. Tidal marshes contain channel networks that often have complex morphologies (Rinaldo et al., 2004). These channel networks control the movement of water, sediment, and solutes into and out of tidal marsh

systems. Therefore, changes in tidal channels due to vegetation growth and sea level rise can be important factors in tidal marsh equilibrium. Global climate change may have significant impacts on plant species composition, growth heights, the duration of the growing season, and the amount of winter die-back (vegetative minima), particularly in the mid-Atlantic region. The effect of plant growth in channels on velocity and discharge into tidal wetlands is not well studied and the ability of various submerged aquatic vegetation (SAV) species to reduce the cross sectional mean velocity is not well defined (Wilson, 2007). Therefore, existing hydrodynamic models of flow and sediment transport in tidal channels are poorly constrained due to the lack of data on vegetative roughness (Lawrence et al., 2004).

The purpose of this research is to evaluate flow hydraulics in a tidal marsh network with extensive *Hydrilla* growth. Tidal flow into a marsh network is constrained by the discharge through the tidal channel cross section at the mouth. Discharge is the product of average velocity and cross sectional area. Velocity was measured during maximum SAV conditions (July –October) when SAV reduces the effective cross sectional area and provides the maximum influence on flow resistance, velocity and discharge.

1.2 Hypotheses

I. At maximum growth heights, *Hydrilla* growing on the channel bed will significantly increase flow resistance and thus reduce tidal channel velocities in Patuxent river marshes.
II. The hydraulic consequences of flow resistance caused by *Hydrilla* can be observed in both the at-a-station and downstream hydraulic geometry equations. The equations for velocity, during maximum *Hydrilla* growth, will be significantly different from both theoretical values and measurements from other tidal systems.
III. The hydraulic consequences of *Hydrilla* on channel velocities will decrease travel distances (length= velocity*tidal half-period). As a result, for most tidal cycle conditions, travel distances for water and sediment will be significantly less than the total length of the channel network.

Previous Work

2.1 Boundary layer theory and its application to vegetated channels

Fluid flow can be divided into two regions, the main flow region that has small velocity gradients, and a boundary layer where velocity gradients and viscous stresses are large. In this main flow region, flow is approximately two-dimensional and the Navier-Stokes equation for fluid motion can be simplified (Prandtl, 1952). The Prandtl-von Karman Law of the Wall can be expressed as:

$$\frac{\bar{u}}{u^*} = \left(\frac{1}{\kappa}\right)\ln\left(\frac{Z}{Zo}\right)$$

where κ is von Karman's constant, Z is relative height above the bed, Zo is the height above the bed where the velocity is zero, ū is mean cross sectional velocity, and u* is shear velocity (Wang et al., 1993). Von Karman's constant is defined as:

$$\kappa = \left(\frac{u^*}{Z}\right) \Big/ \left(\frac{\delta u}{\delta Z}\right)$$

where u* is shear velocity, Z is relative height above the channel bed, and δu/δZ is the rate of change of local velocity with respect to height above the bed (Prandtl, 1952). Von Karman's constant is experimentally derived and ranges from 0.38-0.41. For water flows with low sediment concentrations, the constant is usually taken to be 0.40 (Bradshaw and Huang, 1995; Nepf and Ghisalberti , 2008). The shear velocity is defined by:

$$u^* = \sqrt{gSH}$$

where S is the energy gradient, g is the acceleration due to gravity, and H is the average water depth.

For many geophysical boundary layers such as stream flow or the atmospheric boundary layer, the velocity profile is logarithmic (Prandtl, 1952). The local velocity (u) is proportional to the logarithm of the distance (Z) above the channel bed (Carollo et al., 2002). In wetlands where channels contain extensive patches of submerged vegetation, the velocity profile commonly shows three layers (Figure 1). A zone with logarithmic velocity profiles may exist above the vegetation boundary layer. The shear velocity for this upper flow region can be described as:

$$u^{*'} = \sqrt{gS\left(H - Z_m\right)}$$

where Zm is the height of the plane of momentum absorption (Nepf and Ghisalberti, 2008). The plane of momentum absorption is the height above the bed where the vegetation absorbs the energy from turbulent fluid flow; this is shown by a rapid change in velocity. Nepf and Ghisalberti (2008) further explain that the plane of momentum absorption has a thickness they define as $(aC_D)^{-1}$, where C_D is the drag coefficient and *a* is the density of the canopy. The thickness of the plane of momentum is representative of the stress- and potential-driven layer as seen in Figure 1. This plane of momentum layer and the roughness sub-layer make up the middle of the three layers.

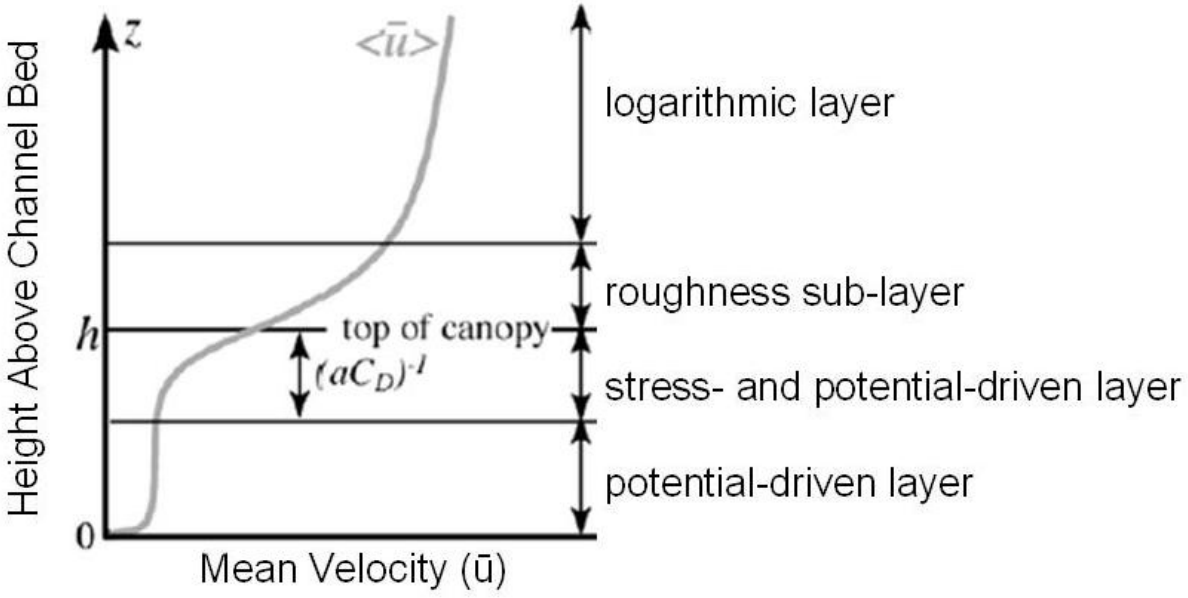

Figure 1: Mean velocity profile showing the layers of submerged vegetation flow. Upper layer is logarithmic, middle layers show rapid change and increase in velocity, lower layer shows low velocities. The top of the canopy (h) is equivalent to Zo and the height of the plane of momentum (Zm). $(aC_D)^{-1}$ is the thickness of the

deflected vegetation. Stress-driven refers to turbulent and dispersive stresses whereas potential-driven refers to the water surface gradient. (Image modified from Nepf and Ghisalberti, 2008)

The lower layer of the velocity profile is driven by potential gradients, also referred to as water surface gradients (Nepf and Ghisalberti, 2008). The potential gradients produce extremely low velocities and the velocity of flow in this region is assumed to be close to zero. The implication of this assumption is that most of the flow into a tidal channel is above the vegetative roughness layer, which significantly reduces the effective cross sectional area used to calculate discharge.

Earlier work by Carollo et al. (2002) also supports this three layer flow for vegetated channels. They describe the concavity of the velocity profile to be concave down with a vertical asymptote as ū/u* approaches zero. The middle layer shows a rapid increase in velocity values with an inflection point at the height of maximum roughness. This maximum roughness is considered the height of the vegetation. Carollo et al. (2002) go on to describe the upper layer as having a concave-up velocity profile. The concavity supports the idea that the inflection point is within the middle layer and has physical implications with respect to the channel vegetation.

In this study, the height of the plane of momentum (Zm), the height of the vegetation (h) and the height at which velocity is zero (Zo) are all considered to be equivalent. Therefore, I assume a two layer flow during vegetated conditions. Thus, the layer above the vegetation is assumed to contain all of the significant flow and the layer below the vegetation is assumed to contain no significant flow. It is recognized that a small amount of water will flow through the vegetation; however, the velocities will be so low due to the already low velocities above the vegetation.

2.2 Laboratory and modeling experiments of vegetative roughness

The effect of vegetation on channel flow resistance has been evaluated through flume experiments and modeling exercises. Several groups of scientists including Carollo et al. (2002), Lawrence et al. (2004), Rinaldo et al. (2004), Wilson (2007) and Wu et al. (1999) have conducted research on the effect of vegetation on flow resistance. Carollo et al. (2002) used a rectangular laboratory flume with a turf bottom containing three varieties of grasses. The density and height of the stems were measured and an acoustic-doppler velocimeter was used to measure local flow velocities (Carollo et al., 2002). Carollo et al. (2002) found that velocity distributions remained logarithmic and exhibited three vertical zones with an inflection point that is dependent on the height of the vegetation. This finding is in agreement with Nepf and Ghisalberti (2008). Carollo et al., (2002) also found that the density of the vegetation had little effect on the shape of the velocity distribution.

Wilson (2007) used artificial and real grass in a laboratory flume to determine relationships among Manning's n, vegetal drag-Reynolds number, vegetation height and flow depth. The vegetal drag (C_D') is defined as:

$$C_D^{'} = \lambda C_D = \frac{2gS}{\bar{u}^2}$$

where C_D is the drag coefficient, λ is the vegetal area fraction per unit length of channel, g is the acceleration due to gravity, S is the water surface gradient and ū is mean cross sectional velocity. The Manning equation relates average velocity to depth (H), gradient (S), and a roughness

coefficient (n). This coefficient can be determined if the other parameters in the equation are measured:

$$n = \frac{(H^{0.67} S^{0.5})}{\bar{u}}.$$

Note the similarity of this equation to the equation for shear velocity. Manning's roughness, n, is inversely proportional to ū. The roughness parameter ū /u*′ is preferred because it is dimensionless:

$$\frac{\bar{u}}{u^{*'}} = \frac{\bar{u}}{\sqrt{gS(H - Zm)}}.$$

Wilson (2007) concluded that as flow depth (H) increases, Manning's n decreases. Wilson (2007) also states that the vegetal drag-Reynolds number is strongly correlated to the height of vegetation. Wilson (2007) based his study methods on Wu et al. (1999) who studied vegetative roughness using a horsehair mattress to simulate channel vegetation. Wu et al. (1999) also conclude that as flow depth increases, Manning's n decreases asymptotically to a constant. The results of these experiments suggest that flow resistance should decrease with lower vegetative heights.

Lawrence et al. (2004) used a hydrodynamic model to simulate tidal flow. The model was developed using RMA-2 v. 4.3., which is a finite element code that simulates the flow of water through simplification and solution of the Navier-Stokes equation. Model requirements include depth of water, downstream and cross-stream velocities, Manning's roughness coefficients, magnitude of eddy viscosity, tidal cycle and tidal range. The numerical inputs were estimated based on previous research. There are however, few data on roughness and eddy viscosity, therefore, these parameters must be estimated, which greatly limits the reliability of the model results. Lawrence et al. (2004) used values of Manning's n ranging from 0.07 to 0.50. These values are up to an order of magnitude higher than average terrestrial values (n = 0.035). In their study, they found that an increase in roughness resulted in a lag in peak discharge during flood tide and a decrease in the magnitude of peak discharge during ebb tide.

Bathymetric data and aerial imaging were used by Rinaldo et al. (2004) to explore geomorphic characteristics of four different marshes. Rinaldo et al. (2004) note that at the Pagliaga salt marsh in Venice, Italy, flow resistance greatly reduces the amplitude of normal tidal oscillation and over the past ten years there has been a decrease in the overall length of the channel network. The decrease in length could be a result of decreased flow travel distances.

The experiments described above use laboratory flumes, simulations, and the use of tidal gauge data and geomorphic data from aerial photographs. Few of these experiments involve direct flow resistance measurements, but these studies do provide a framework for field studies and help explain why field studies are necessary to constrain flow resistance in tidal channels.

2.3 At-a-station hydraulic geometry

The hydraulic characteristics of stream and tidal channels can be summarized by using empirical hydraulic geometry equations. Hydraulic geometry, introduced by Leopold and Maddock (1953), are power law equations, based on the continuity equation, which describes the relationships of width, depth and velocity to discharge:

$$w = aQ^b \qquad d = cQ^f \qquad \bar{u} = kQ^m$$

where w is water surface width, d is mean depth, ū is mean velocity, Q is discharge, a, c and k are coefficients and b, f and m are exponents. Hydraulic geometry equations can be used to describe hydraulic adjustments to discharge at different points in a channel network (known as downstream hydraulic geometry) or it can be used to describe the changes in hydraulic variables with increasing discharge at one cross section, which is termed at-a-station hydraulic geometry. The continuity equation provides the following relationships (Leopold and Maddock, 1953):

$$Q = area \cdot velocity = w \cdot d \cdot \bar{u} = (aQ^b)(cQ^f)(kQ^m) = (a \cdot c \cdot k)(Q^{b+f+m})$$

$$Q = (a \cdot c \cdot k)(Q^{b+f+m})$$

Therefore:

$$b + f + m = 1 \text{ and } \quad a \cdot c \cdot k = 1$$

The exponents for the power functions, b, f and m, represent the rates at which width, depth and velocity increase with discharge at a particular station. These exponents are very useful when studying tidal settings because discharge varies continuously over diurnal tidal cycles.

In a recent analytical study of hydraulic geometry, Dingman (2007) discusses the relationships among channel shape, hydraulic geometry exponents and coefficients. Dingman (2007) proposes that the channel shape is constrained by:

$$Z^* = Y_m^* \left(\frac{2}{W^*} \right)^r x^r, \; 0 \le x \le \frac{W^*}{2}$$

where Z* is the height of the channel bed above the lowest channel elevation, x is the horizontal distance from the center of the channel, Y_m* is the maximum bankfull depth and W* is the bankfull width. The shape is represented by the exponent r; as r increases the channel moves from a triangular, to parabolic, to rectangular shape. These changes in shape can be expressed on a b-f-m ternary diagram, as seen in Figure 2 (Rhodes, 1977; Dingman, 2007).

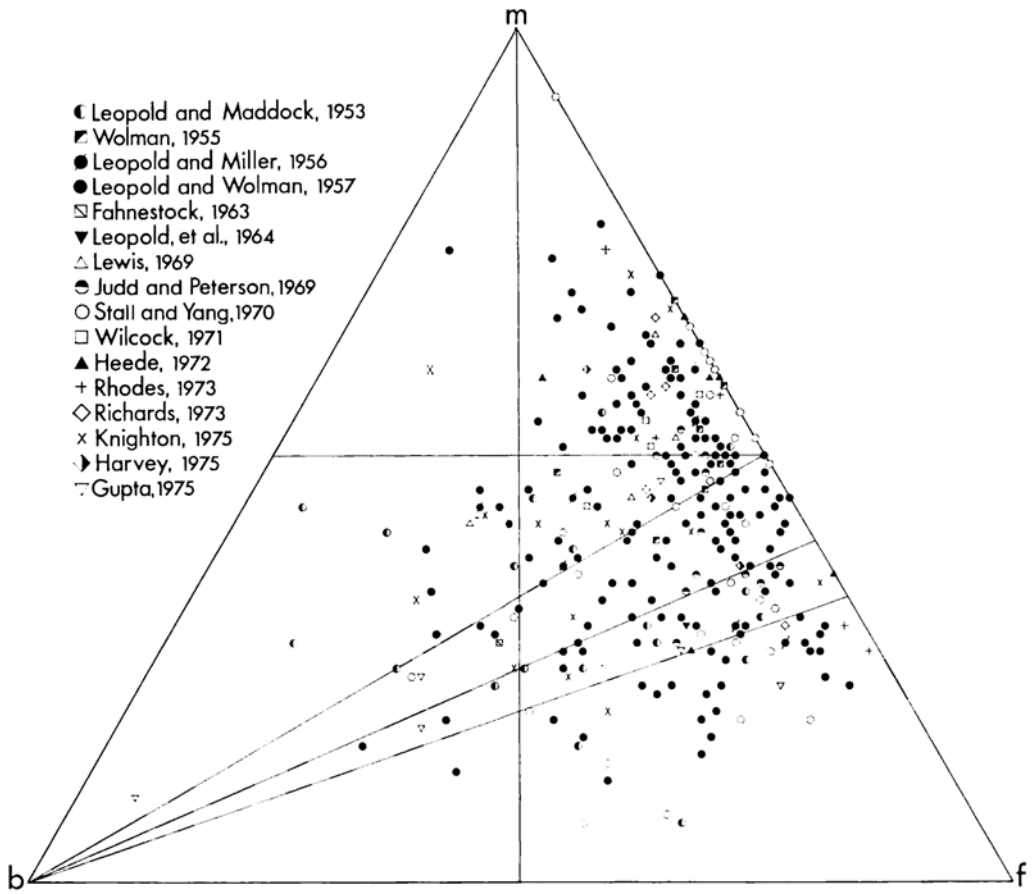

Figure 2: By continuity, at-a-station hydraulic geometry exponents can be plotted on a b-f-m ternary diagram. This ternary diagram shows 315 hydraulic geometry data sets compiled by Rhodes (1977).

Flow resistance equations express velocity as a function of channel depth, gradient, and roughness coefficients. Depth, gradient, and velocity can be described as power functions of discharge; therefore roughness coefficients can also be expressed as power functions for the at-a-station hydraulic geometry case. If flow resistance remains constant, velocity will increase as depth and gradient increase. Dingman (2007) expressed these equations as:

$$\bar{u} = K \cdot d^{p} \cdot S^{q}$$

where K is a general resistance coefficient, d is mean depth, S is slope, p is 1.00 and q is 0.50, The depth of flow in a channel is a function of channel shape as well as discharge. Dingman (2007) derives an estimator, ř, for the shape exponent in the channel shape equation defined as $Z^* = Y_m^* \cdot (2/W^*)^{r} \cdot x^{r}$ for $0 \le x \le W^*/2$. He defines this estimator using the width and depth exponents (b and f respectively) of hydraulic geometry to be:

$$\check{r} = \frac{f}{b}.$$

During summer months, vegetation occupies a significant volume of the channel. Therefore, the effective cross section is a subset of the total cross sectional area. If SAV height is approximately constant in a channel system, then the amount of the channel area occupied by

vegetation should be larger for upstream portions of the channel system. This should affect both the at-a-station and downstream hydraulic geometry and the shape factor in different parts of the channel system.

2.4 Downstream hydraulic geometry

Downstream hydraulic geometry examines the changes in width, depth and velocity with discharge in stream or tidal networks. In tidal channels, discharge decreases from the mouth to upstream locations. The exponents, b, f and m, represent the rates at which width, depth and velocity change within the tidal network. Previous studies of tidal marshes have shown that the width constricts in tidal systems, which maintains the average velocity and brings water and sediment deep into the tidal networks. Therefore, the hydraulic geometry exponents are smallest for velocity and greatest for width as discharge decreases from the network mouth to interior tidal channels (Langbein, 1963; Myrick and Leopold, 1963).

Original work on estuary morphology was conducted by Pillsbury (1956), as presented in Langbein (1963). Pillsbury defined the exponential decrease in width upstream from the network mouth as:

$$w = w_o e^{-jy\cot\varphi}$$

where w is the bankfull water surface width at a distance y upstream, w_0 is the network mouth bankfull width, φ is the lag between the time of maximum slope and the time of maximum velocity, and j is defined as:

$$j = \frac{\alpha}{\sqrt{gH}}$$

where α is the mean angular speed of the lunar tide, H is mean bankfull water depth at distance y upstream and g is the acceleration due to gravity. For the semidiurnal lunar tide, Pillsbury states that α =0.00014 radians per second. Langbein (1963) argues that this exponential relationship along with the geometry for the tidal channel allows for the determination of theoretical "downstream" hydraulic geometry exponents, including the change in gradient with discharge (*z*). Langbein (1963) suggested that river networks, including terrestrial and tidal systems, tend toward a uniform energy distribution and minimum work. Friction (flow resistance) and the volume of the tidal prism determine the amount of work done by the tide (Langbein, 1963). A minimization of the work done during ebb and flood, affects the depth and velocity. Langbein's hydraulic analysis of Pillsbury's hypothesis results in the following relationship between *f*, the depth exponent, and z, the slope hydraulic exponent:

$$z = -\frac{f}{2}.$$

Langbein (1963) uses the assumed constraints of uniform energy distribution and minimum energy expenditure to derive theoretical values for *b*, *f*, *m* and *z*. He then tests these values with field data and finds that his theoretical values were within 0.01 of field values (see Table III). The relationship between *z* and *f* is used in this study to determine the exponent for slope (energy gradient) in the tidal network. If z is small, within 0.05 of zero, then the water surface gradient can be assumed constant throughout the network, at bankfull conditions.

Study Site and Methods

3.1 Study site

Field research was conducted at the Patuxent Wetlands Park located in Lothian, Maryland in Anne Arundel County. The study site is constrained to the interior marsh located along the west bank of the Patuxent River upstream of the Route 4 Bridge. This network marsh was chosen as the study site because of its location within the freshwater portion of the Patuxent River and its morphology. Sea level rise causes tidal influences and the salt wedge to move further upstream; this can transform freshwater wetlands into salt marshes (Tiner, 2005). This wetland is one of the most northern wetlands along the Patuxent River and therefore it is at the upstream end of the tidal system.

The morphology of this wetland constrains the hydraulic fluxes into the marsh network, which makes it a great study site for this project. The natural levees (seen in Figure 3) prevent river flow from overtopping into the marsh along the boundary with the main Patuxent River. The levees also funnel tidal flow through the channel mouth, which makes it easier to measure total flux of water into the marsh network.

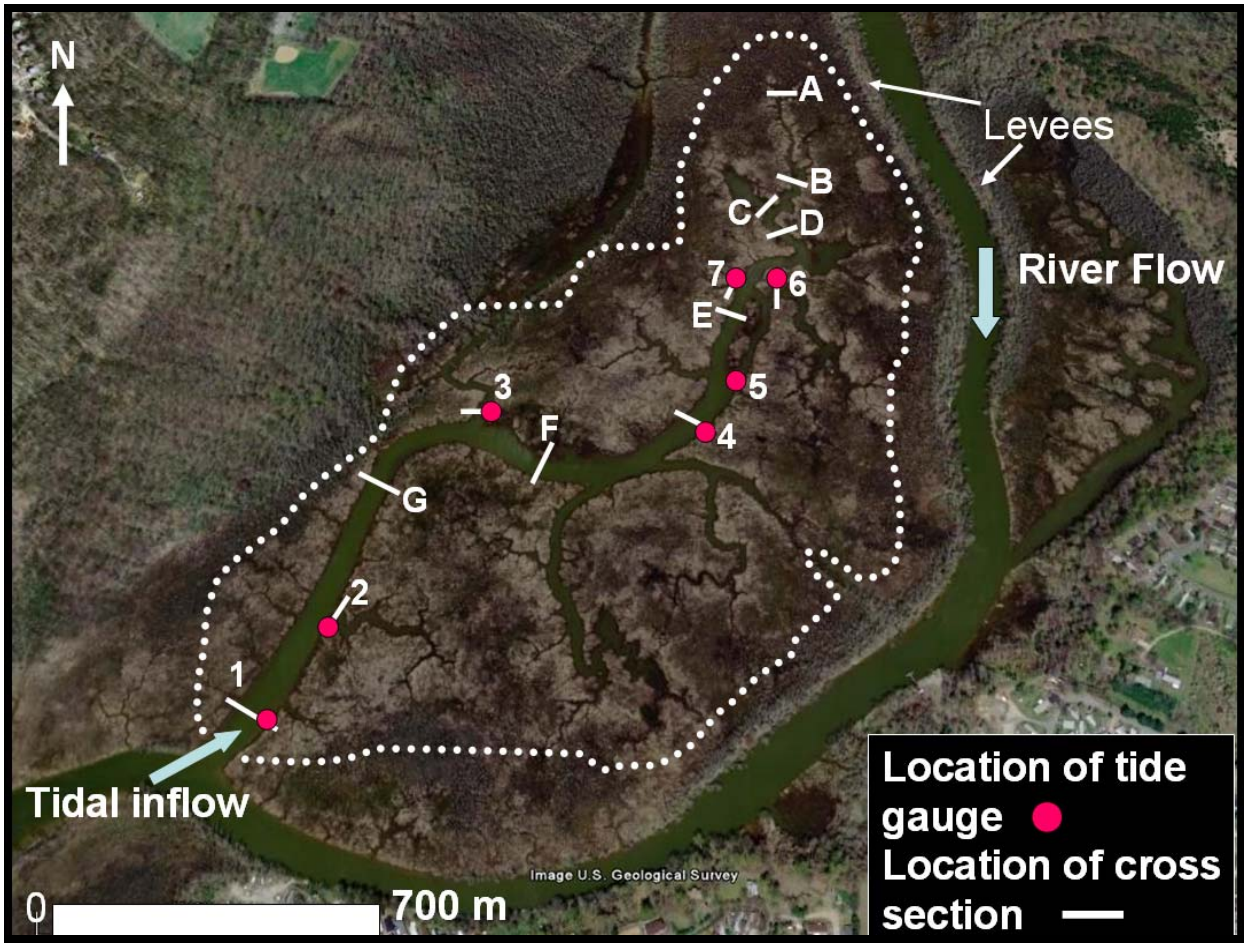

Figure 3: The entire study site is restricted to the area within the white dotted line. Measurements were taken at gauge and cross section locations. The direction of river flow, tidal flow and location of natural levees are clearly labeled. (March 2007 image by US Geological Survey accessed through Google Earth)

3.2 Design of field experiments

In the Chesapeake region, tides follow a semi-diurnal cycle; there are two high and two low tides during each lunar day (Figure 4). The two high tides and low tides, however, have daily inequity, meaning that they are never consecutively at the same height. A full tidal period starts and ends at any given peak or trough; for example a tidal period will last from the first high tide of the day to the next high tide of the day.

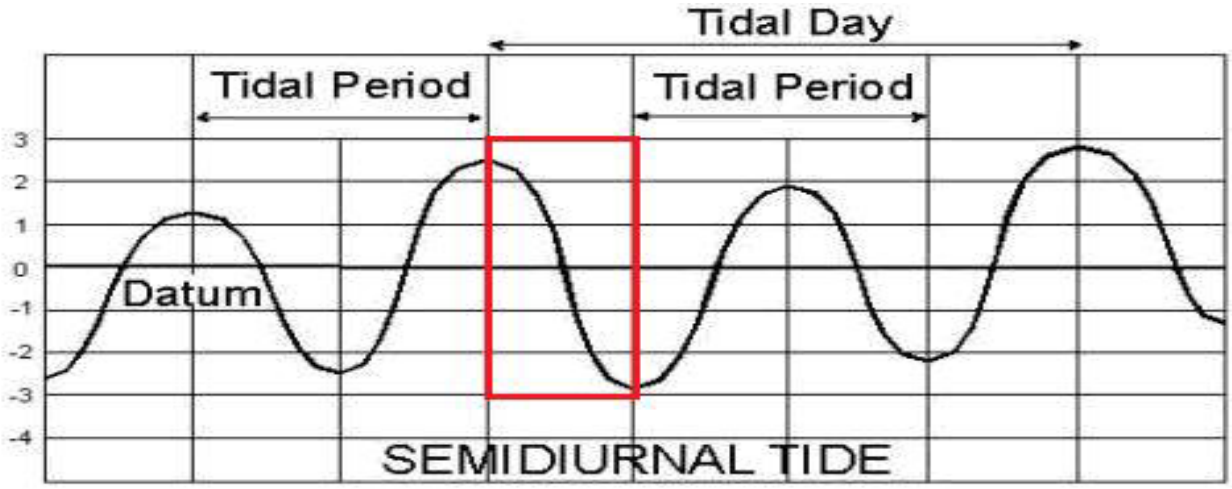

Figure 4: A semi-diurnal tide has two high and two low tides each lunar day. High tides and low tides are not equivalent each day. Typically, the largest high tide occurs during a full moon. The red box indicates the half-tidal period when field experiments were carried out. The y-axis is height above and below an established datum equal to zero. (Image courtesy of the U.S. Department of Transportation, 2006)

Field experiments were conducted during half a tidal period, from the higher high tide to low tide (Figure 4). Data collection was initiated at the field site before high tide so that initial tidal stage measurements can be made at slack tide, before the channels begin to drain. At slack tide, the local water surface is horizontal; initial measurements such as surface width and cross sectional depth measurements can be made or referenced to this condition (Figure 5). Depth measured at slack tide is measured from a horizontal surface. Thus, we are measuring from a standard and hence reducing measurement errors.

Research was conducted during ebb, rather than flood so that gravity wave equations could be used to evaluate flow resistance. Water surface gradient measurements also become much easier to measure during ebb and previous studies show similar flow characteristics for ebb and flood tides (Myrick and Leopold, 1963). In order for the tide to drain, the downstream must drain first; this gravity wave pull creates a surface water gradient that can be easily measured during ebb tide conditions. Measurement sites are shown in Figure 3.

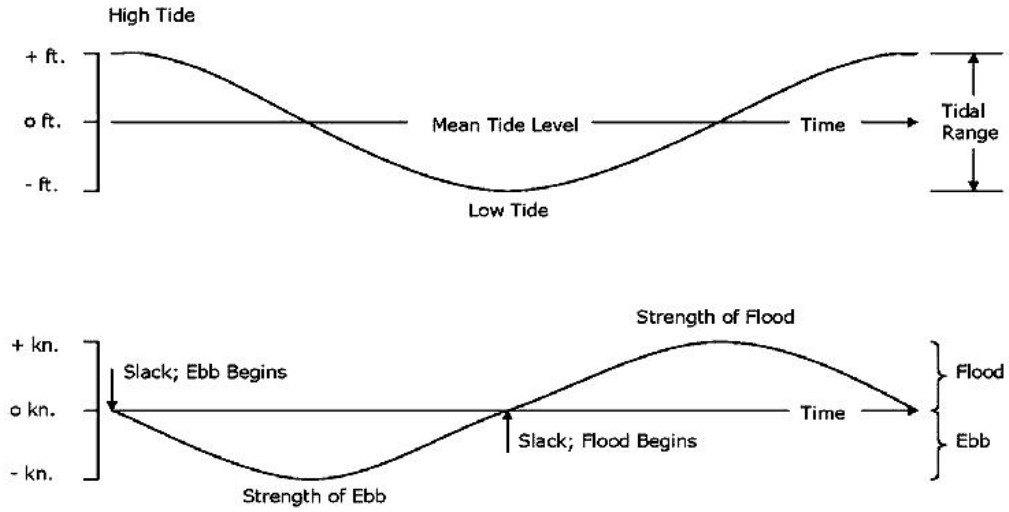

Figure 5: At high tide velocity goes to zero and the water surface is horizontal. Velocity reaches its peak magnitude half way between high and low tide. At low tide the velocity goes to zero and the water surface becomes horizontal again. When the flow reaches high tide or low tide it is referred to as slack; this denotes zero velocity and a horizontal water surface. (Image from Hicks, 2006)

The design of this project was to collect a suite of field measurements during maximum *Hydrilla* growth and abundance (July –October). Measurements were made during monthly high tides on the following dates (see Table I).

Table I: Dates, Tides and Measurements during Field Experiments

Date	Site #: Measurements	High / Low	Tide Time	Height (m)	Sunrise / Sunset	Moon	Time
07/07/09	1: V, S, A 2: V, S, A 3: V, A	High Low High	6:29 AM 2:15 PM 6:36 PM	1.25 0.40 0.79	5:49 AM 8:35 PM	Set Rise	5:50 AM 8:59 PM
08/07/09	6: V, A 7: A	Low High Low High	1:13 AM 7:08 AM 2:29 PM 7:34 PM	0.40 1.19 0.34 1.01	6:14 AM 8:11 PM	Set Rise	7:42 AM 8:52 PM
10/11/09	4: V, A, S 5: S	Low High Low	7:31 AM 11:37 AM 6:06 PM	0.40 0.79 0.27	7:13 AM 6:34 PM	Set	2:41 PM
11/20/09	A: V, 2: S 4: V, A	Low High Low High	3:13 AM 7:17 AM 1:32 PM 8:06 PM	0.23 0.58 0.01 0.99	6:54 AM 4:50 PM	Set Rise	8:00 PM 10:24 AM
04/03/10	A: V, A 1: V, S 2: S 4: V, A	Low High Low High	3:13 AM 7:17 AM 1:32 PM 8:06 PM	0.23 0.58 0.01 0.99	6:54 AM 4:50 PM	Set Rise	8:00 PM 10:24 AM

Measurement Key: V: velocity, S: energy gradient, A: cross sectional area
For site numbers and letters see Figure 3. Tide information for Hills Bridge (Rt. 4), Lothian, MD provided by Maryland Department of Natural Resources Fisheries Service, accessed 2009 - 2010

3.3 Measurement of hydraulic variables under field conditions

In the field, tidal stage, width, depth, and velocity were measured directly using tidal gauges, tape measures, and current meters. Procedures for measurements of these parameters are described below.

3.3.1 Tidal stage

Tidal stage was recorded from a staff gauge (Figure 6) that was placed perpendicular to the water surface at slack tide. The maximum tidal gauge reading was recorded at slack tide; tidal gauge height was recorded at 5-10 minute intervals. Gauge height is plotted against time to yield a diagram of tidal stage as a function of time (Figure 7).

Figure 6: Tidal stage is measured with a staff gauge

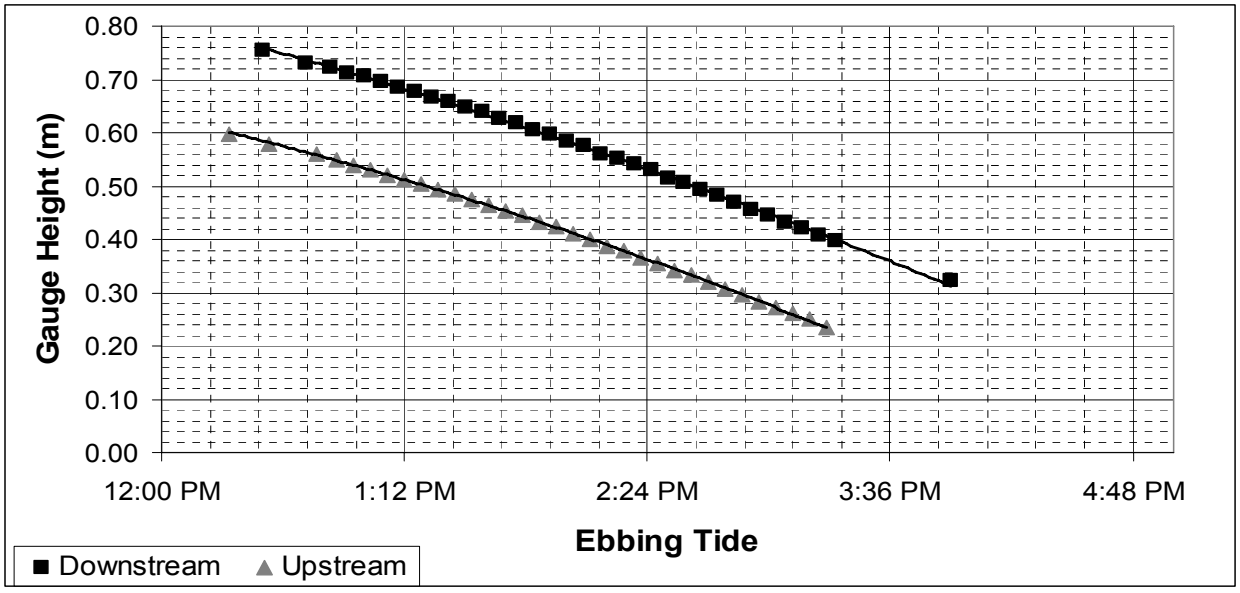

Figure 7: This graph shows the raw gauge height data over time for two staff gauges. Quadratic functions fit to these data and are used to determine gauge height at any time over the measured range of tidal period. Gauge data are standardized to an initial start value and corrected gauge height functions are used to calculate water surface gradient. The error bars for these data are smaller than the data points.

3.3.2 Cross sectional area

In the field, the surface width was measured at high tide. During slack tide, the depth was measured at meter intervals across the channel. These measurements are illustrated in Figure 8. Using the midsection method, outlined by the United States Geological Survey (USGS), the total cross sectional area is determined by first sectioning the width so that a rectangle is formed around each depth measurement (Buchanan and Somers, 1969). As seen in Figure 8, the area of a small rectangle is the product of the small width the depth it surrounds. The total cross sectional area is the sum of all of these small rectangles. Accurate measurement of channel cross section requires measurement of sufficient verticals in a cross section to obtain an accurate cross section measurement. Although the number of measurements to define the cross section depend upon cross section complexity, 15-20 measurements within a simple channel are sufficient to define the channel within 2% of its value (this is supported by the Central Limit theorem and has been experimentally verified for Maryland channels by Kosiba, 2008).

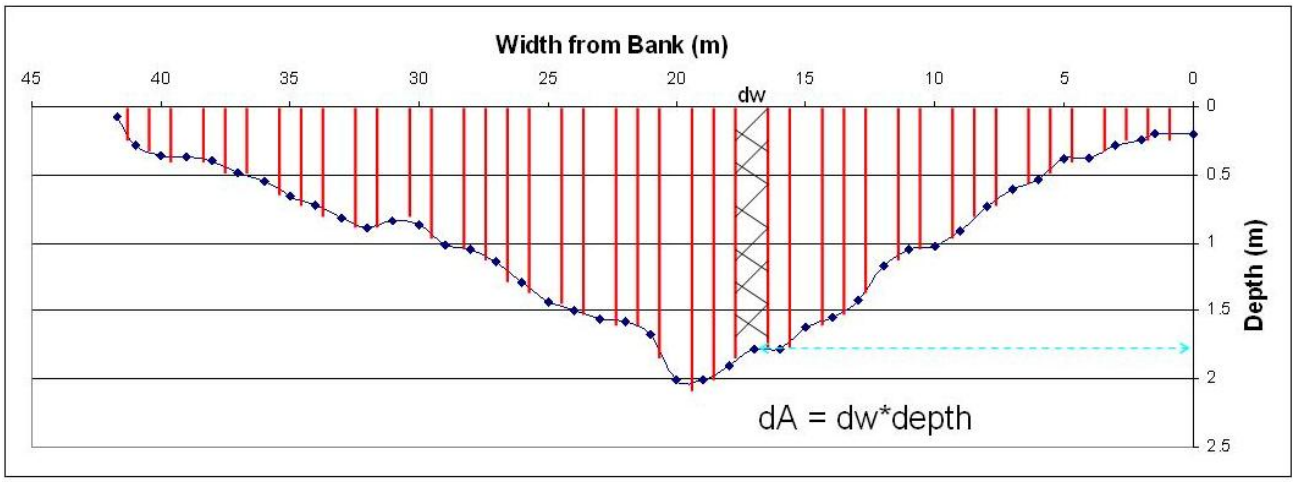

Figure 8: This figure demonstrates how to calculate cross sectional area. Between each depth measurement the width is divided so that equal width is between each depth measurement. This sectioning is indicated by the red bars and dw. The area (dA) of the small rectangle is dw*depth, where depth can be read off the graph. The total cross sectional area is the sum of each small rectangular area: $A = \sum dA$.

3.3.3 Average and maximum velocity

In open channel flow, most velocity profiles are logarithmic above the boundary layer. As previously described, velocity above vegetated layers is often logarithmic, but velocity within the vegetative layer is not. Most of the discharge, however, moves above the vegetative boundary layer. To estimate average velocity, enough measurements need to be made to define the flow structure. For this project, these measurements were made as follows. Within each vertical profile, the maximum (surface) velocity and the approximately zero vegetative boundary layer (Zm) velocity were measured. These two measurements were made across the channel at a given gauge height. At several locations, additional vertical measurements were made to determine velocity profiles (Figure 9). These measurements were used to determine the velocity profile for each vertical, as well as providing a direct measurement of Zm. These measurements

were used to determine average velocity within each vertical profile. If the velocity profile is logarithmic, the two measurements (Zm and maximum velocity) in each vertical profile can be used to determine the average velocity.

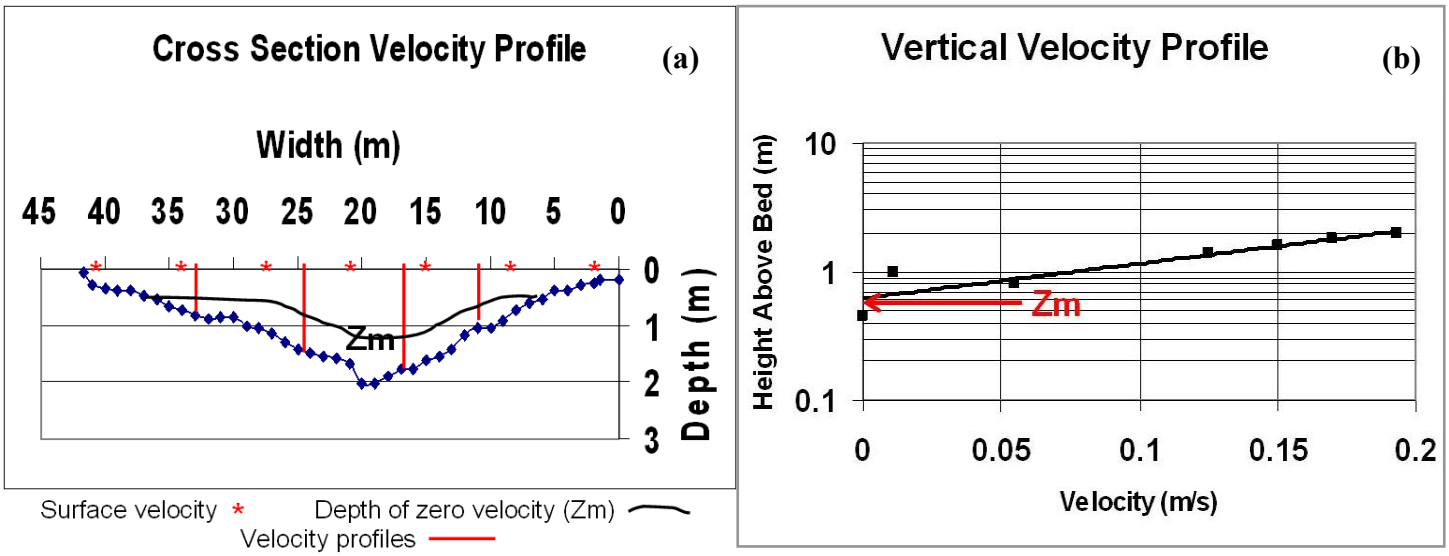

Figure 9a-b: (a) This figure shows where velocity profiles and surface velocities are measured. Also, in this figure the height of Zm is indicated. (b) This height is determined by the vertical velocity profile shown on the right; the height of the vegetation is at the height above the bed that the velocity goes close to zero.

Discharge for the cross section was determined by finding the average velocity for each vertical section, then multiplying average velocity by area for each rectangle of flow and summing these values over the cross section:

$$Q_{total} = area_1 \cdot u_1 + area_2 \cdot u_2 + area_3 \cdot u_3 \ldots = \sum area_i \cdot u_i$$

The USGS recommends the vertical-velocity curve method to determine discharge and states that each vertical velocity should be made so that less than ten percent of the discharge lies between each vertical measurement site (Buchanan and Somers, 1969). This means that more measurements should be made at the center where depths are higher rather than spacing vertical sites equally across the channel. Average velocity was then calculated from the discharge calculation:

$$Q_{total} / A_{total} = \text{average velocity}$$

For tidal channels, it is very difficult to measure velocity profiles quickly enough across the channel to characterize each point on the tidal stage-velocity diagram. Chen and Chiu (2002) studied the relationship between maximum and average velocity. Assuming symmetry of a cross section, they found that just a few measurements along a vertical axis could yield a ratio between the mean cross sectional and maximum velocities. Chen and Chiu (2002) studied different magnitudes of discharge and found that for a given cross section there is a constant and stable linear relationship between mean cross sectional velocity and maximum velocity. Their method of determining mean cross sectional velocity is particularly applicable to tidal channels where the velocity distribution changes rapidly with time. Therefore, in this study, average velocity is estimated by continuous measurement of the maximum velocity in the cross section over time

and the development of a relationship between average velocity (ū) and maximum velocity (U) is given by (Chen and Chiu, 2002):

$$\overline{u} = U \cdot \phi$$

where ϕ is the ratio of average to maximum velocity for the cross section. The linear relationship between cross sectional area and gauge height is used to calibrate the linear relationship between average velocity and maximum velocity for a given cross section (Figure 10). Through the assumption of a logarithmic layer above the vegetation, the ratio of mean cross sectional velocity to maximum velocity (□) has been determined so that ū = 0.4292U for the site shown in Figure 10.

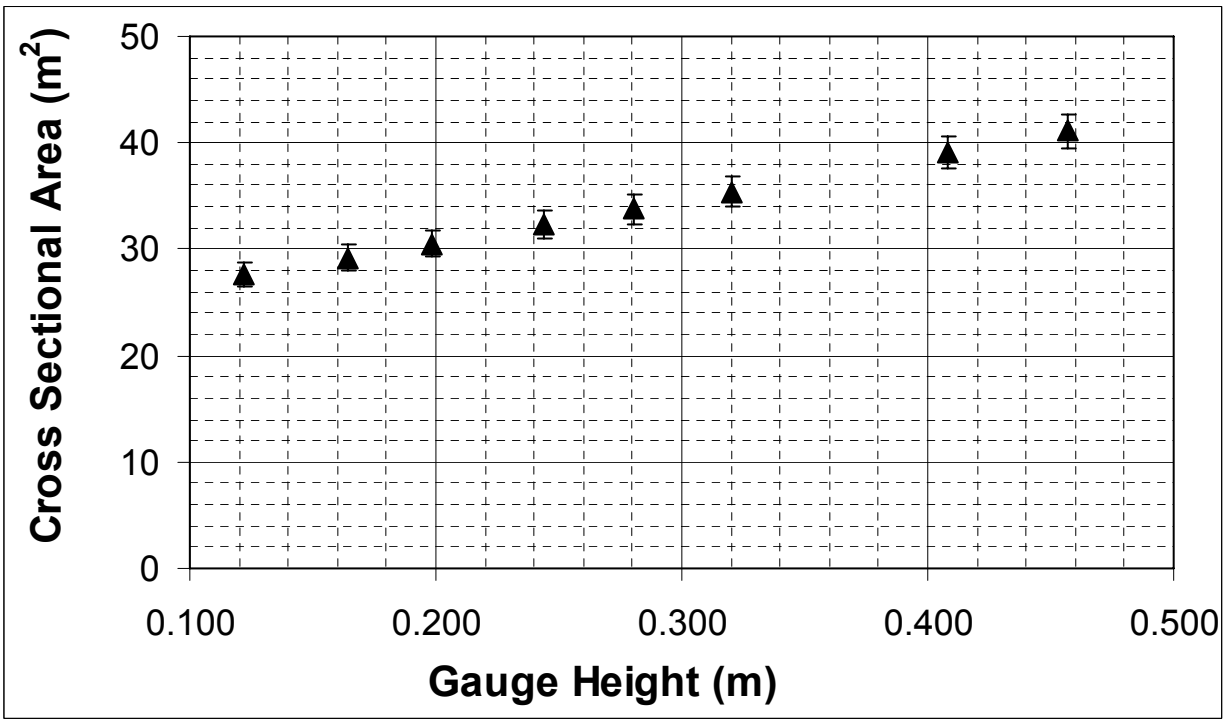

Figure 10: The relationship between cross sectional area and gauge height is linear. This suggests that the channel shape does not change significantly and that there is a constant relationship between average velocity and maximum velocity. The error bars show a 4% error for the cross sectional area; the error bars for the gauge height are smaller than the data points.

3.4 Data analysis

Data analysis includes calculation of water surface (energy) gradient, flow resistance and both at-a-station and downstream hydraulic geometry. The methods of data analysis are described in detail in the following sections.

3.4.1 Water surface (energy) gradient

The water surface gradient was determined from two tide gauges. At slack tide, the water surface is horizontal. The tide drains as a gravity wave; therefore, there is a larger drop in gauge height downstream than there is upstream. This difference in the gauge height drop between the

two tide gauges is used to calculate water surface (energy) gradient (Figure 11). The length between the upstream and downstream locations is measured to ±1 m over distances of 100 to 200 m.

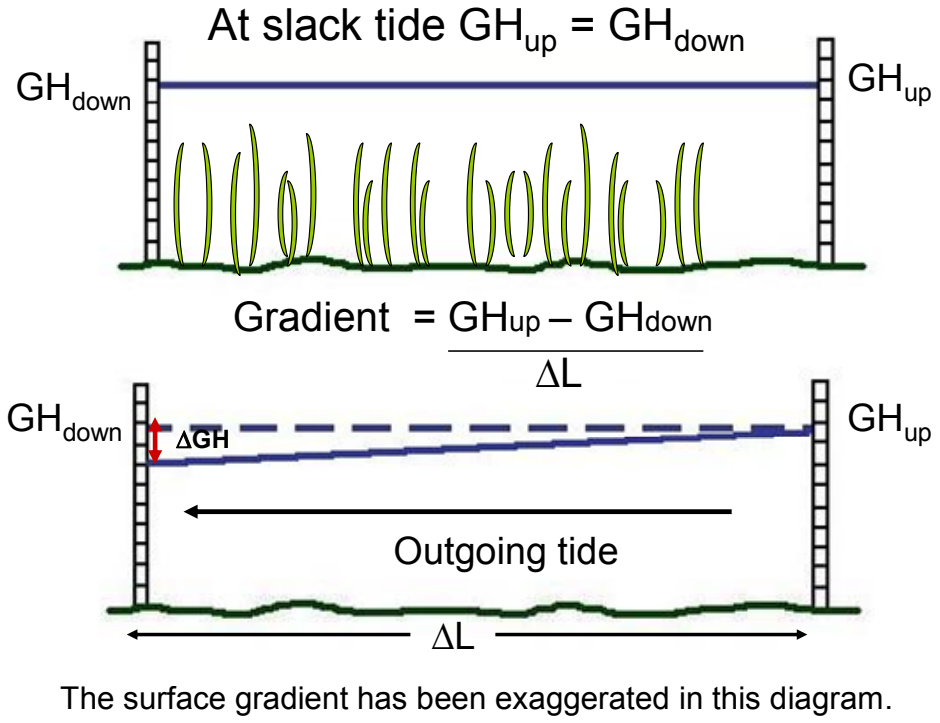

Figure 11: Energy gradient is calculated from the change in gauge height between an upstream gauge (GH_{up}) and a downstream gauge (GH_{down}) at the same point in time. The difference in gauge height is divided by the measured distance between the two locations to determine the water surface gradient, which is the energy gradient if the width is constant.

3.4.2 Flow resistance

The resistance that the vegetation creates in the channel is quantified by the roughness equation:

$$\frac{\bar{u}}{u^{*'}} = \frac{\bar{u}}{\sqrt{gS(H - Zm)}}$$

where ū is mean velocity, g is the acceleration due to gravity, H is mean water depth, S is the water surface gradient, Zm is the height of the plane of momentum absorption, and u*´ is vegetative shear velocity.

3.4.3 Hydraulic geometry

At-a-station hydraulic geometry, as described above, involves measuring width, depth and velocity over a half-tidal cycle and plotting these hydraulic variables against discharge (Figures 12a-c). The exponents of the power equations are the slopes of each respective line; the slopes b, f and m describe the amount of change in width, depth and velocity that occurs with a change in discharge.

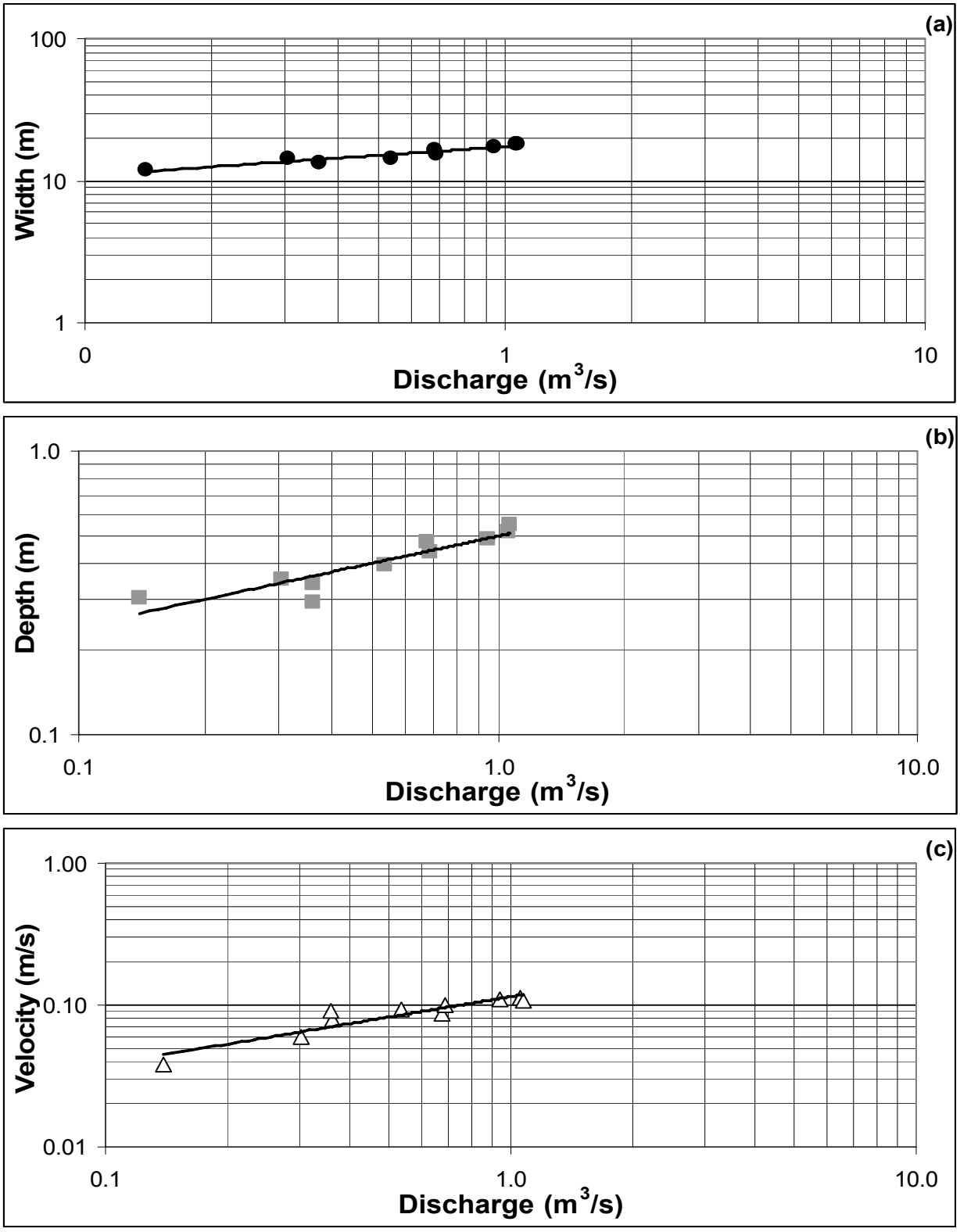

Fig 12a-c: Presentation of at-a-station hydraulic geometry for site 2. (a) The relationship between width and discharge for this cross section is $w = 17.4Q^{0.20}$. (b) The relationship between depth and discharge for this cross section is $d = 0.50Q^{0.32}$. (c) The relationship between velocity and discharge at this cross section is $\bar{u} = 0.12Q^{0.48}$. The power equations are valid by continuity: 0.20 + 0.32 + 0.48 = 1.00 and 17.4*0.502*0.115 = 1.0.

Downstream hydraulic geometry is the set of power laws determined when discharge is plotted against width, depth and mean velocity. In contrast to at-a-station hydraulic geometry, downstream hydraulic geometry presents the changes in width, depth and velocity that occur within channel networks for a single event or condition (usually the bankfull discharge). Therefore, the slopes b, f and m describe the amount of change in width, depth and velocity within the tidal network (from headwaters to mouth). For this study, sites were selected along the main tidal channel, and the surface width, average depth and mean velocity were plotted against the bankfull discharge for each site. In this study, bankfull discharge is defined as the discharge that fills the entire channel, up to the marsh platform. Due to the morphology of tidal networks, the largest discharge will indicate the site near the mouth, whereas the smallest discharge will correspond to the most-upmarsh (interior) site.

Although hydraulic geometry exponents are initially fit by least squares regression, the equation is constrained by continuity: $b + f + m = 1.00$, which constrains the sum of the exponents (slope of the power functions). Additionally, the coefficients of power equations are also constrained by continuity so that $a \cdot c \cdot k = 1.0$. Furthermore, for any discharge, the product of w $\cdot$ d $\cdot$ ū from the power equations must equal the discharge. These three considerations constrain the position of the equations.

3.5 Error Analysis

All measurements were collected in such a way as to reduce error. Equipment was set up prior to high tide so that at slack tide, when the surface of the water is horizontal, there was a datum associated with each day's measurements. Gauge height is recorded to the minute and therefore has a time interval error of ± 1 minute. The staff gauges used for gauge height, are marked with increments of a hundredth of a foot and can be read to a thousandth of a foot with a ± 0.01 ft error. Therefore, the error in recording gauge height is ± 0.002 m.

The error associated with cross sectional area is dependent on width and depth. Soft-sediment on the bed can add an additional source of error in the vertical measurements. Depth is taken to have an error of ± 0.04 m. Measurement of the width has a measurement error of ± 0.04 m, but wind and measuring tape stiffness can add to width error. For large channels, such as the mouth of this network, the width can be measured accurately to a tenth of a meter, so that $\sigma_w = \pm$ 0.1 m. By error propagation, for the network mouth, $\sigma_A = \pm 1.14$ m^2 or $\sigma_A < 4.0\%$ error. Shown below are the steps of error propagation:

$$A = w \cdot d$$

$$\sigma_A^2 = \left(\sigma_w \left(\partial A/\partial w\right)\right)^2 + \left(\sigma_d \left(\partial A/\partial d\right)\right)^2$$

$$\sigma_A^2 = \left(\sigma_w \cdot d\right)^2 + \left(\sigma_d \cdot w\right)^2$$

$$\sigma_A = \sqrt{\left(\sigma_w \cdot d\right)^2 + \left(\sigma_d \cdot w\right)^2}$$

$$\sigma_A = \sqrt{\left[\left(\pm 0.04m\right) \cdot \left(0.84m\right)\right]^2 + \left[\left(\pm 0.04m\right) \cdot \left(37.72m\right)\right]^2}$$

$$\sigma_A = \pm 1.14m^2 \ : \ 3.56\%$$

The error on the velocity measurement is dependent on both the type of velocity meter that is used to make the measurement and the range of velocity values. The calibration of the Swoffer Model 2100 Current Velocity meter provides velocity values within ± 1% error for velocity readings above 0.20 m/s. When velocities readings are below 0.20 m/s, the error becomes larger. If velocity readings are below 0.20 m/s but above 0.01 m/s, the error is 2%. The major error in determination of average velocity from velocity profile readings comes from three parameters. The first parameter is identification of Zm, the second parameter is the assumption of logarithmic velocity profiles where it is not logarithmic and the third parameter is the relationship between maximum velocity and average velocity.

The error associated with calculation of energy gradient is dependent on the distance between the two staff gauges and the gauge height. The length between the upstream and downstream locations is measured to ± 1 m over distances of 100 to 200 m. The gauge height is measure to ± 0.002 m. Therefore by error propagation $\sigma_S = \pm 3 \cdot 10^{-5}$ m/m.

Error for vegetative flow resistance (u/u*′) depends on error for gradient, mean channel depth, determination of Zm and mean channel velocity. By error propagation $\sigma_{\bar{u}/u^{*\prime}} = \pm 0.1$ which translates to a 1.4% to 3.1% (1σ) error. All measurements were collected in accordance with USGS guidelines and therefore were collected to minimize error.

Results

4.1 At-a-station hydraulic geometry

At-a-station hydraulic geometry were analyzed for five cross sections; these sites show variations in exponents from the mouth to upmarsh locations (see Table II for all at-a-station hydraulic geometry variables). Three of these spatially distributed sites were chosen to be graphically represented so that a relationship between hydraulic exponents and distance upstream can be better understood (Figures 13a-c).

Table II: At-a-station Hydraulic Geometry Exponents and Coefficients: Patuxent Tidal Channels

Site #	1	2	3	6	7
Distance upstream (m)	**59**	**236**	**557**	**1097**	**1097**
Exponent b (width)	0.27	0.20	0.04	0.01	0.01
Exponent f (depth)	0.27	0.32	0.56	0.02	0.29
Exponent m (velocity)	0.46	0.48	0.40	0.97	0.70
Coefficient a (width)	30.1	17.4	15.0	10.6	6.6
Coefficient c (depth)	0.66	0.50	0.54	0.44	0.51
Coefficient k (velocity)	0.050	0.12	0.12	0.21	0.30
Shape factor (f/b)	1.0	1.6	14	2.0	29
b + f + m	1.00	1.00	1.00	1.00	1.00
a*c*k	1.0	1.0	1.0	1.0	1.0

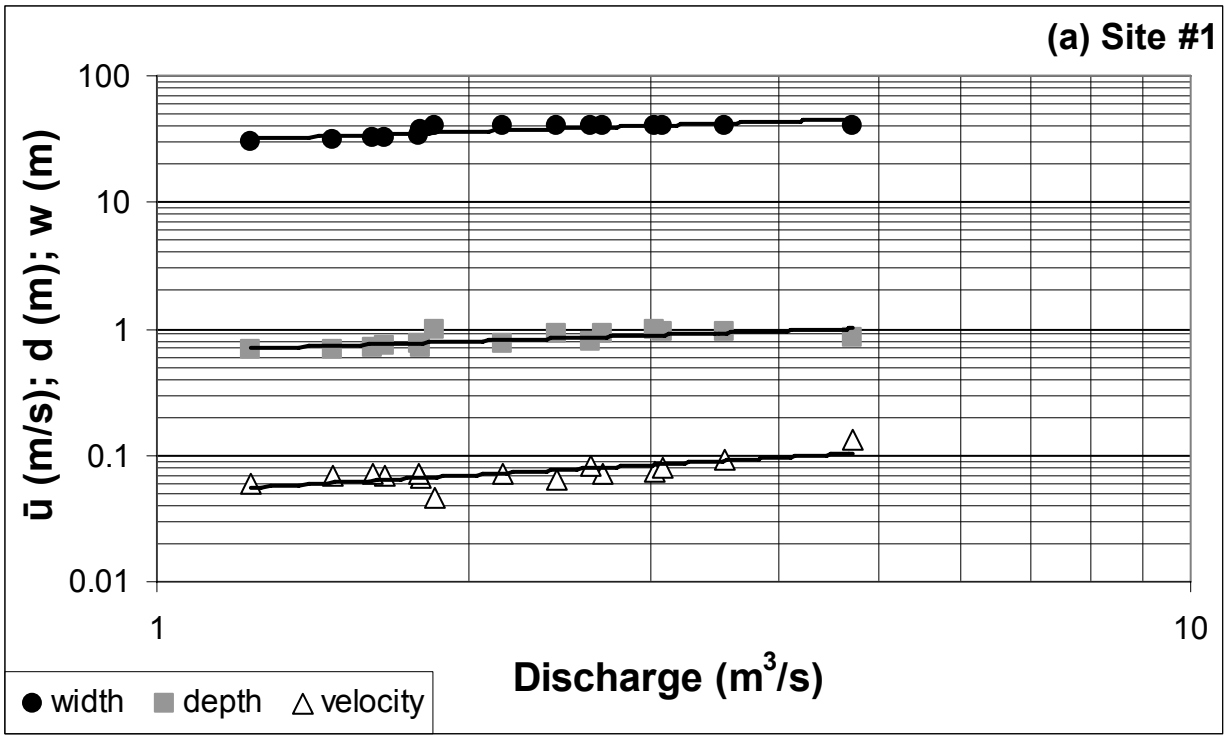
(a) Site #1
100
10
1
0.1
0.01
ū (m/s); d (m); w (m)
1
10
Discharge (m3/s)
width
depth
velocity

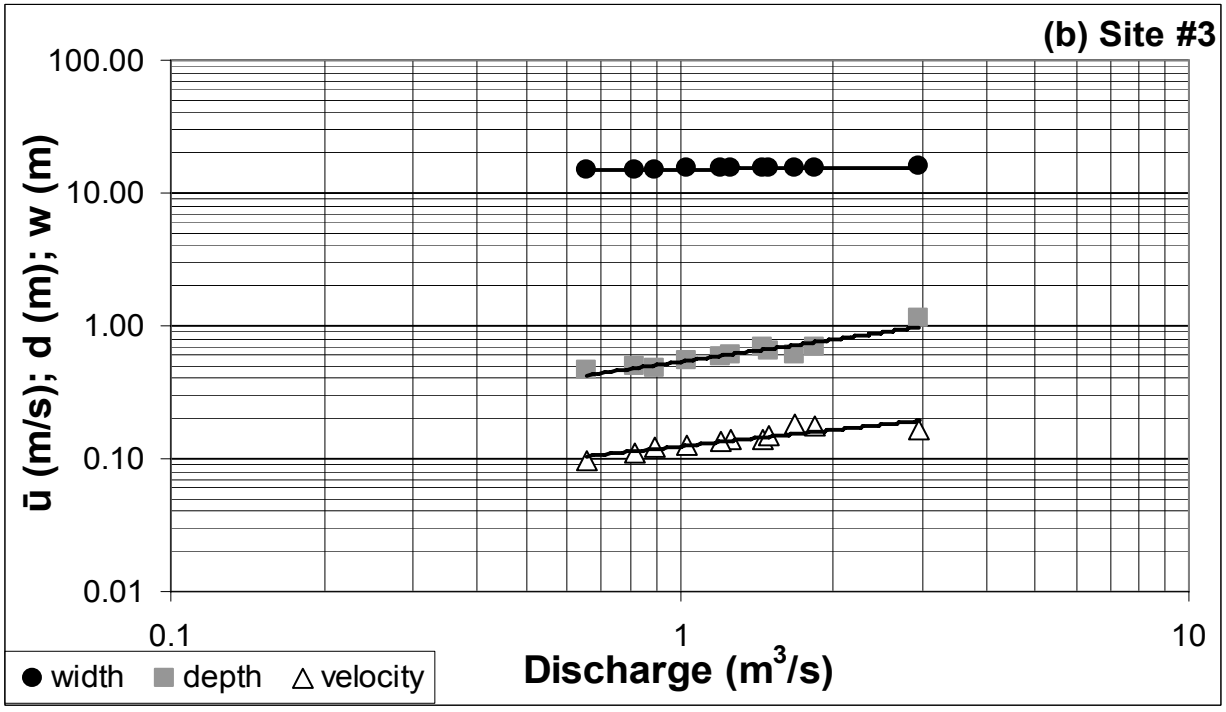
(b) Site #3
100.00
10.00
1.00
0.10
0.01
ū (m/s); d (m); w (m)
0.1
1
10
Discharge (m3/s)
width
depth
velocity

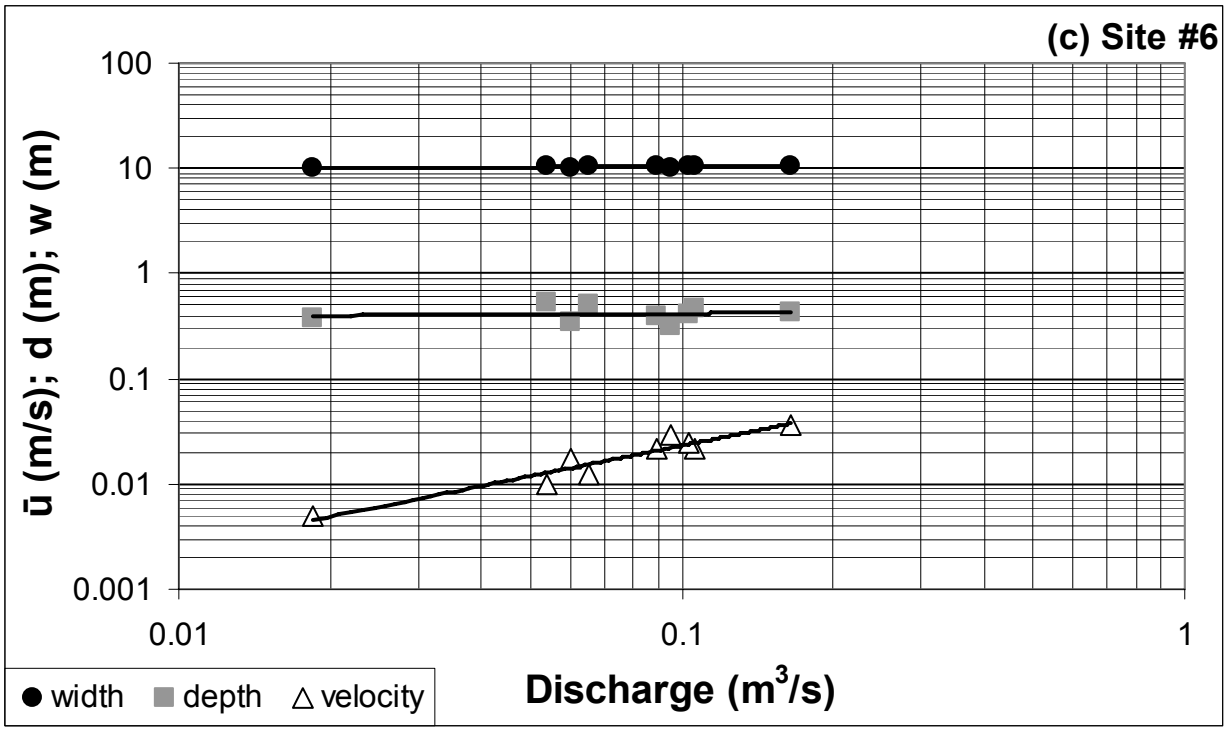

Figure 13a-c: At-a-station hydraulic geometry for three different sites ranging from downstream near the network mouth to upstream past the midpoint of the tidal system. The velocity exponents increase two-fold beyond the midpoint of the system. (a) Site 1 is furthest downstream and has the following hydraulic relationships: $w = 30.1Q^{0.27}$, $d = 0.66Q^{0.27}$, and $\bar{u} = 0.050Q^{0.46}$. (b) Site 3 is located further upstream (~ 500 m upstream from site 1). This site has the following hydraulic relationships: $w = 15.0Q^{0.04}$, $d = 0.54Q^{0.56}$, and $\bar{u} = 0.12Q^{0.40}$ (c) Site 6 is the most upstream site (~1040 m from site 1 and ~540 m from site 3) and has the following hydraulic relationships: $w = 10.6Q^{0.01}$, $d = 0.44Q^{0.02}$, and $\bar{u} = 0.21Q^{0.97}$. Note that each of the sets of exponents and coefficient respectively, sum and multiply to unity (see Table II).

Site 1 is located downstream, closest to the network mouth, site 6 is located upstream beyond the midpoint of the total network length and site 3 is located between site 1 and 6.. Comparison of these three sites show the velocity exponent (*m*) drastically increasing beyond the midpoint of the network. At this location, and similarly at site 7, vegetation moderately clogs the channel during bankfull flow. As the flow approaches low tide the water level drops to the height of the vegetation and the entire channel is filled with vegetation. This reduces the region of flow above the vegetation to zero and hence the velocities begin to approach zero. This observation supports the original assumption of a no flow region below the vegetation.

As previously discussed, Rhodes (1977) placed more than 300 data sets on a b-f-m ternary diagram to gain insight into the typical geometry of river channels. Dingman (2007) expanded on this concept by creating two boundaries. The first boundary contains high concentrations of hydraulic geometry data and the other boundary contains almost all of the data presented by Rhodes (1977). Cross sections that lie outside of these boundaries could imply that adjustments in parameters in addition to width, depth, and velocity, such as flow resistance, affect the hydraulic geometry relationships. The at-a-station hydraulic geometry exponents for this study have been plotted on Dingman's b-f-m diagram (Figure 14). Two of the sites lie within the highest concentration of data sets, two sites lie within the outer boundary of data sets and one lies far outside of the boundaries.

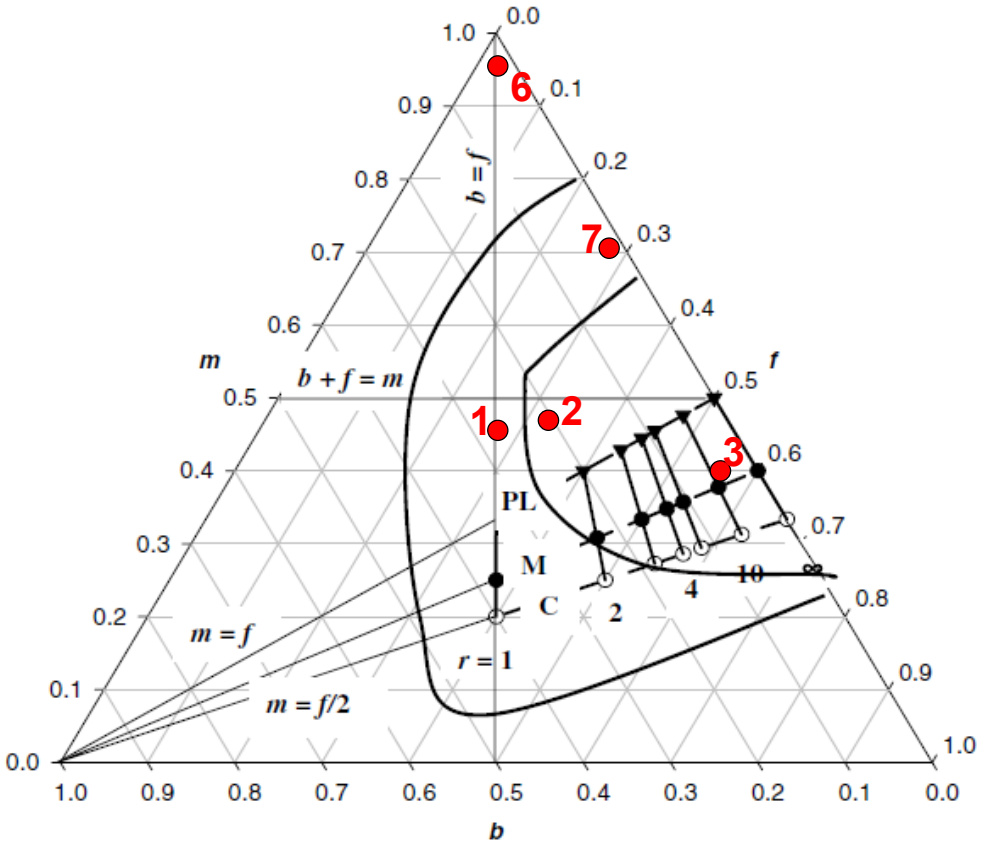

Figure 14: The at-a-station hydraulic geometry exponents for the Patuxent Tidal channels are plotted in red with corresponding site numbers. Dingman (2007) outlined the boundaries of data provided by Rhodes (1977). The inner semi-circular region contains the highest concentration of observed hydraulic exponent values and the outer semi-circular region encapsulates almost all of the values reported by Rhodes (1977). Sites that lie outside of these regions are considered unstable and sites that lie outside of the inner-circle could approach instability. The PL, M and C lines correspond respectively to power-law, Manning, and Chézy hydraulic relations (Dingman, 2007).

The two tributary channel sites, 2 and 3 are contained within the highest concentration of b-f-m data (Figure 14). They have however, very differently shaped channels. According to Dingman's shape factor (ř = *f*/*b*), site 2 is triangular to parabolic, whereas site 3 is very rectangular. Similarly, site 1 and 7 fall within the outer boundary of channel data, but have very different channel shapes. Site 1 (near the mouth) is triangular and site 7 is rectangular. Site 6 plots outside of the boundaries, where *b* is almost equal to *f*, but slightly larger. Rhodes (1977) states that channels that plot in this region tend to show banks that erode more easily than their channel bed. Due to the dense vegetation on the channel bed at this site, if shear velocities are high enough, the banks will erode before the channel bed under vegetated conditions.

At-a-station hydraulic geometry can also be analyzed by evaluating changes in exponents and coefficients as a function of distance into the marsh system. The exponent for velocity (*m*) shows an increase in value in the upstream direction (Figure 15a). This indicates that velocity changes more with discharge at these upstream locations. The channel shape becomes more rectangular upstream, which is indicated by the low values for the width exponent for the upstream sites.

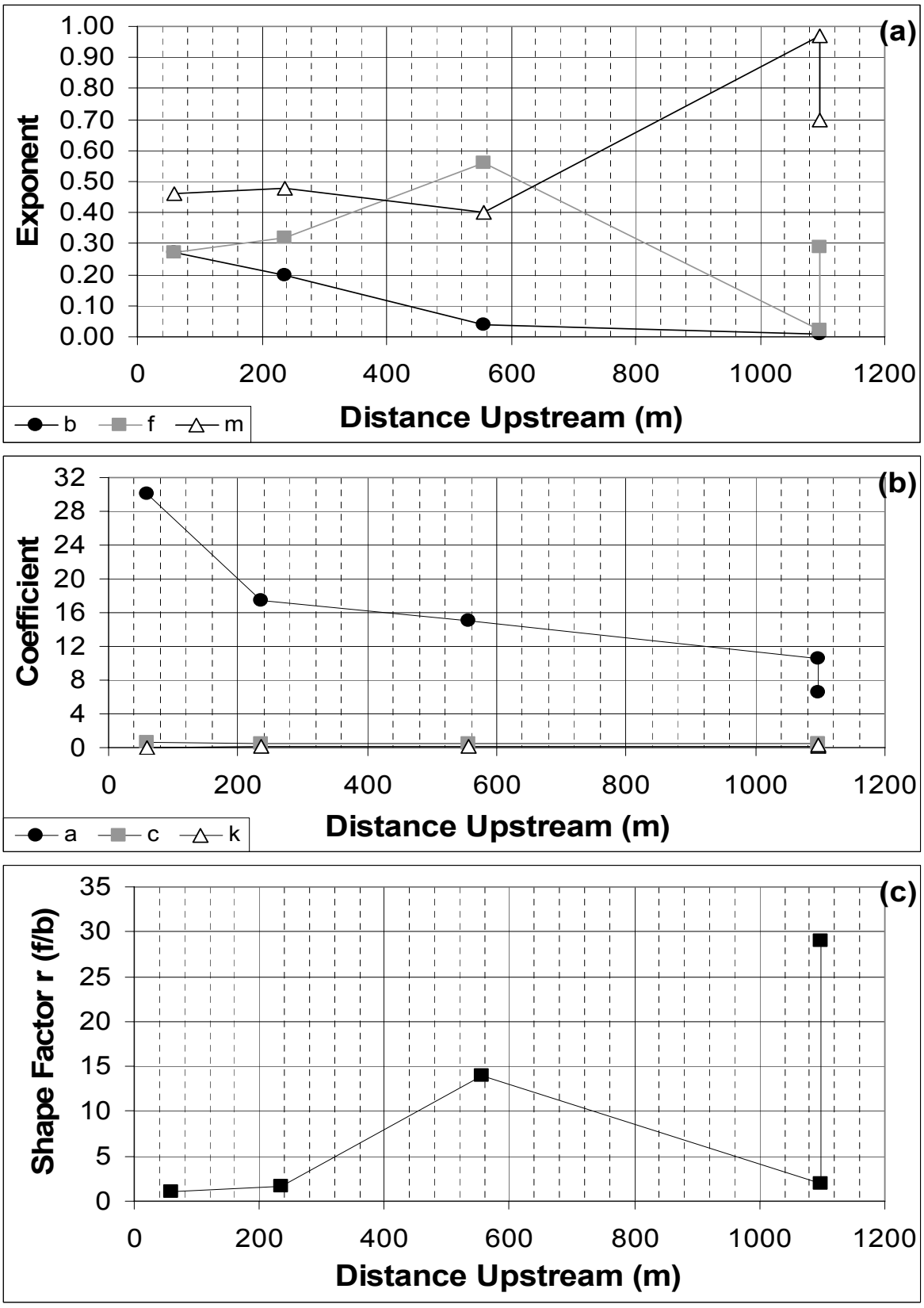

Figure 15a-c: At-a-station exponents and coefficients are plotted against distance upstream to determine any trends in the upstream or downstream direction. (a) Hydraulic geometry exponents show an increase in the

velocity exponent (m), but no trend is expressed for the width and depth exponents. (b) Hydraulic geometry coefficients show a decrease in the width coefficient. The depth and velocity coefficients remain constant in the upstream direction. (c) The shape factor shows an increasing trend upstream, with site 6 as an outlier. The error bars for these data are smaller than the data points and are constrained by the continuity of discharge: $Q = (a*c*k)Q^{b+f+m}$.

The coefficients, *a*, *c*, and *k* also show changes within the tidal network. The *c* and *k* coefficients remain fairly constant, but the coefficient *a* shows a decrease in the upmarsh direction (Figure 15b). Dingman (2007) predicted that as bankfull width increases, *a* would increase and *c* and *k* would decrease. These results support an increase in *a* with and increase in bankfull width, but does not support the latter prediction.

Dingman (2007) examined the implications of channel shape on the hydraulic geometry exponents. Channel shape was evaluated using Dingman's shape factor (ř) which indicates increasing values of ř in the upstream direction (Figure 15c). Site 6 lies outside of this trend; however, site 6 is also the cross section that lies outside of the b-f-m ternary diagram boundary lines.

4.2 Downstream hydraulic geometry

The downstream hydraulic geometry equations determined during vegetative maxima (Figure 16b) are very different from values for other tidal systems, theory, and the estimated values of vegetative minima for the Patuxent channels (see Table III). The exponents during vegetative maxima indicate that width decreases most rapidly upstream, depth remains fairly constant and velocity also decreases upstream. The upstream decrease in "bankfull" velocity is exhibited as a significant value of the exponent *m* during vegetative maxima, whereas most other field and theoretical studies indicate values of *m* close to zero.

The next section provides data on the changes in flow resistance over a tidal cycle at the cross section near the mouth of the tidal creek (see Figure 18c for Manning's n values). These data indicate that the channel was roughest at high tide and became smoother as tidal stage dropped and the vegetation flattened. The lower values of effective Manning's n are around 0.030, very similar to smooth alluvial channels. Therefore, I used the lower values of Manning's n to estimate flow velocities, discharge and "downstream" hydraulic geometry for a condition with minimal SAV. This estimate required use of the Manning equation and an additional assumption that the bankfull water surface gradient for the vegetative minima condition was similar to the vegetated case. The results for this vegetative minima condition are shown in Figure 16c and Table III. In both vegetation conditions, the width decreases most rapidly upstream and therefore the exponent for width (*b*) is the largest of the three exponents. The main differences between maximum and minimum SAV conditions are observed in the velocity exponents and coefficients. The velocity exponent under vegetated conditions triples in value from non-vegetated conditions. When vegetation is at a minimum, the value of the velocity exponent for this study site lies within the range of velocity values (0.00 – 0.09) of other tidal marshes with little to no SAV. The coefficient of velocity *(k*) also significantly changes. Under vegetative conditions, *k* decreases four-fold from non-vegetated conditions. This implies that at any discharge Q, velocity will decrease that Q by a factor of four under vegetated conditions.

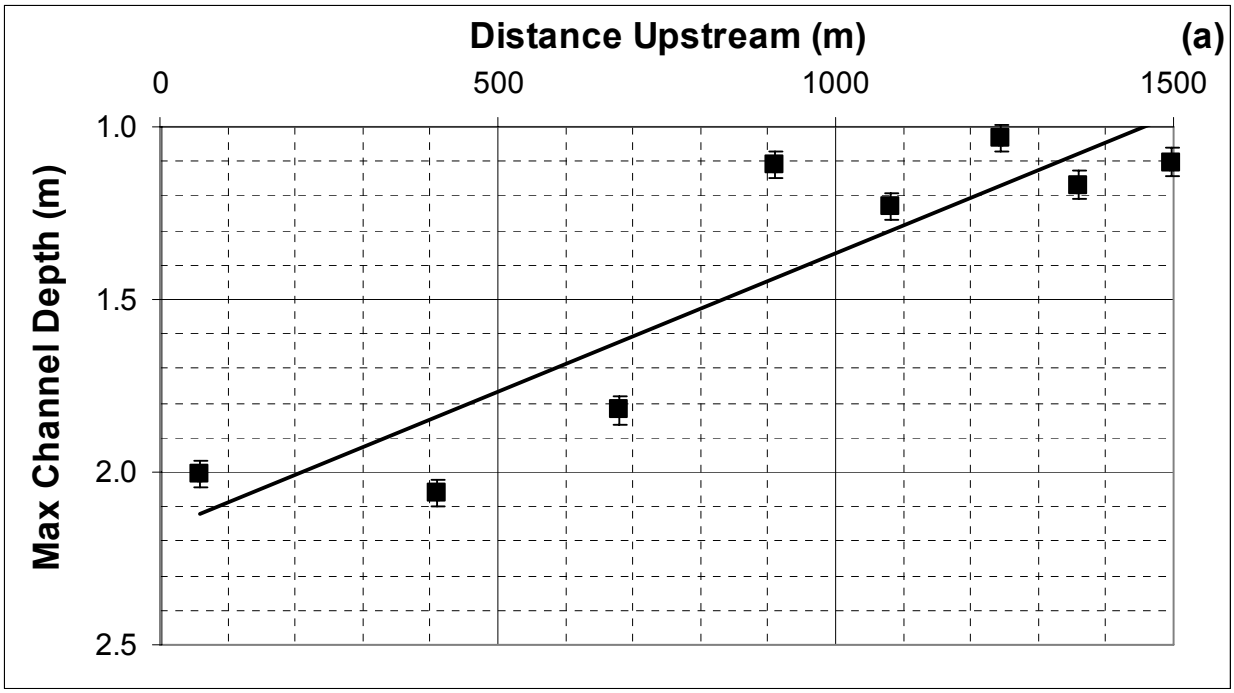
Distance Upstream (m)
(a)
0
500
1000
1500
Max Channel Depth (m)
1.0
1.5
2.0
2.5

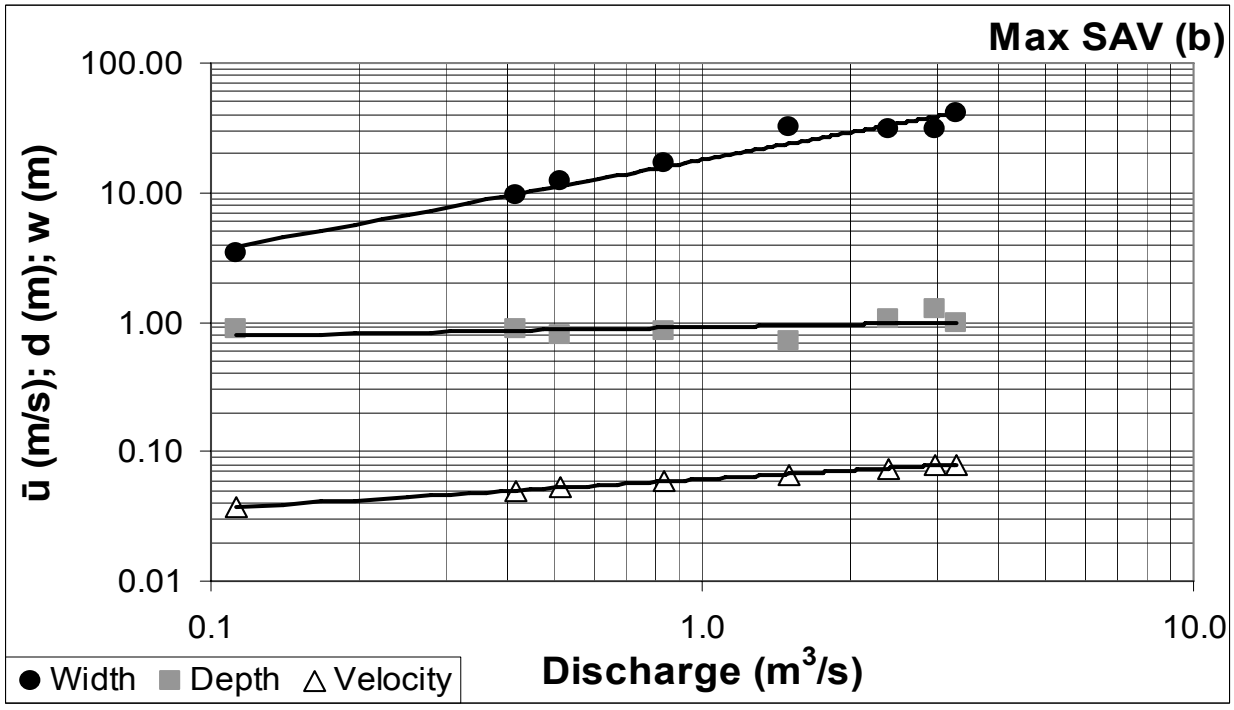
Max SAV (b)
100.00
10.00
1.00
0.10
0.01
ū (m/s); d (m); w (m)
0.1
1.0
10.0
Discharge (m3/s)
Width
Depth
Velocity

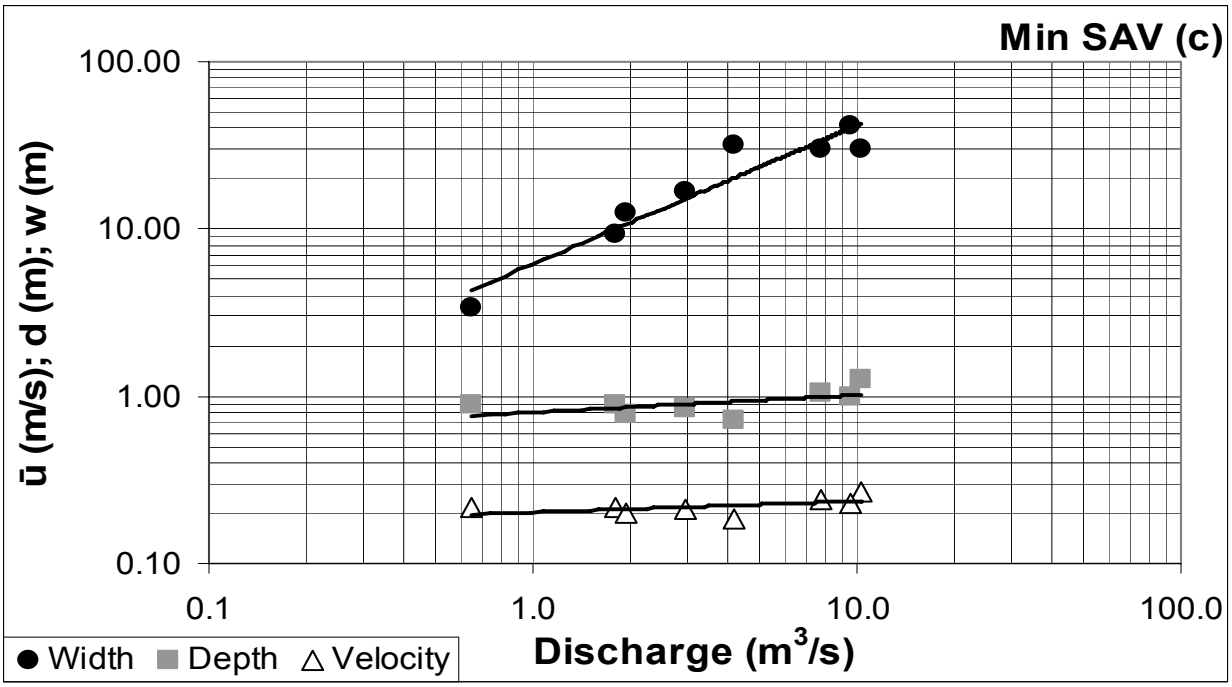

Figure 16a-c: Downstream hydraulic geometry for this tidal marsh during vegetative maxima and minima. (a) Maximum channel depth as a function of distance upstream provides a reference for the average depth used in hydraulic geometry. The total range of maximum depth from up- to downstream is only 1 m. The depth error bars show ± 0.04 m; the error for distance upstream is smaller than the data points. (b) The power equations that relate width, depth and velocity to discharge for the main channel during maximum vegetation are $w = 17.9Q^{0.70}$; $d = 0.92Q^{0.07}$; $\bar{u} = 0.061Q^{0.23}$. Using the continuity of discharge, 0.70 + 0.07 + 0.23 = 1.00 and similarly, 17.9 · 0.92 · 0.061 = 1.0. (c) The power equations that relate width, depth and velocity to discharge for the main channel during minimum vegetation are $w = 6.2Q^{0.83}$; $d = 0.80Q^{0.10}$; $\bar{u} = 0.20Q^{0.07}$. Using the continuity of discharge, 0.83 + 0.10 + 0.07 = 1.00 and similarly, 6.2 · 0.80 · 0.20 = 1.0.

The similarities in downstream hydraulic geometry exponents for the Patuxent SAV minima conditions and other sites and theory, supports the hypothesis that the hydraulic geometry measured during vegetative maxima is due to the influence of SAV on flow structure and flow resistance. These data are compared in Table III.

Table III: Downstream Hydraulic Geometry for Various Tidal Marshes

Hydraulic Exponent		**Patuxent Wetland Park Max SAV (this study)**	**Patuxent Wetland Park Min SAV (this study)**	Wrecked Recorder Creek, VA[1]	Barnstable Marsh, MA[1]	Langbein's Theoretical[2]	Langbein's Unnamed Estuary, VA[2]
width	b	**0.70**	**0.83**	0.77	0.74	0.72	0.72
depth	f	**0.07**	**0.10**	0.23	0.17	0.23	0.22
velocity	m	**0.23**	**0.07**	0.00	0.09	0.05	0.06
slope	z	**-0.035**	**-0.05**			-0.12	-0.10 to -0.17
([1]Myrick and Leopold, 1963; [2]Langbein, 1963)							

The two other field studies reported in Table III are both sites that had little SAV at the time of measurement. The Wrecked Recorder Creek site was located along the Potomac River in Alexandria, Virginia (now the site of Reagan National Airport). The geomorphic study conducted at Wrecked Recorder Creek was conducted in 1960, during a time when the Potomac River had little SAV (Orth and Moore, 1984; Rybicki and Landwehr, 2007). SAV returned to the Chesapeake Bay region in the 1980s; one of the dominant species since that time has been *Hydrilla*, an invasive species to the entire mid-Atlantic region (Hershner and Havens, 2008; Rybicki and Landwehr, 2007). Barnstable Marsh is a salt marsh located in the southwest corner of Cape Cod Bay and contains little to no SAV (Redfield, 1972).

Langbein's (1963) theoretical exponents were derived by analyzing the work done by the tide, assuming uniform energy dissipation along the tidal channel and invoking continuity of discharge. Langbein verified the theoretical hydraulic exponents through a field study of a tidal estuary along the Potomac River. Similar to Wrecked Recorder Creek and Barnstable Marsh, the unnamed estuary in Langbein's study contained no SAV.

Pillsbury (1956) suggested that the decrease in channel width is essential to maintain flow velocity and carry discharge and sediment into the channel (Langbein, 1963). The rapid decrease in velocity even with the appropriate decrease in width suggests another factor (flow resistance) is affecting the flow velocity and thus the total flux of water and energy into this system. The significant upstream decrease in velocity for the vegetative condition suggests that the channel geometry was not formed under the extensive vegetation conditions that we currently see at this marsh.

4.3 Time series data on flow resistance at the mouth of the tidal network

As described in the methods section, flow resistance ($u/u^{*\prime}$) can be calculated from measurements of velocity, energy gradient, and effective depth. Flow resistance and a resistance coefficient (Manning's n) were determined over an ebb tide at the cross section near the tidal mouth. Values of $u/u^{*\prime}$ increase as flow depth decreases during the ebbing tide (Figure 17). An increase in $u/u^{*\prime}$ values indicates a smoothing of the channel.

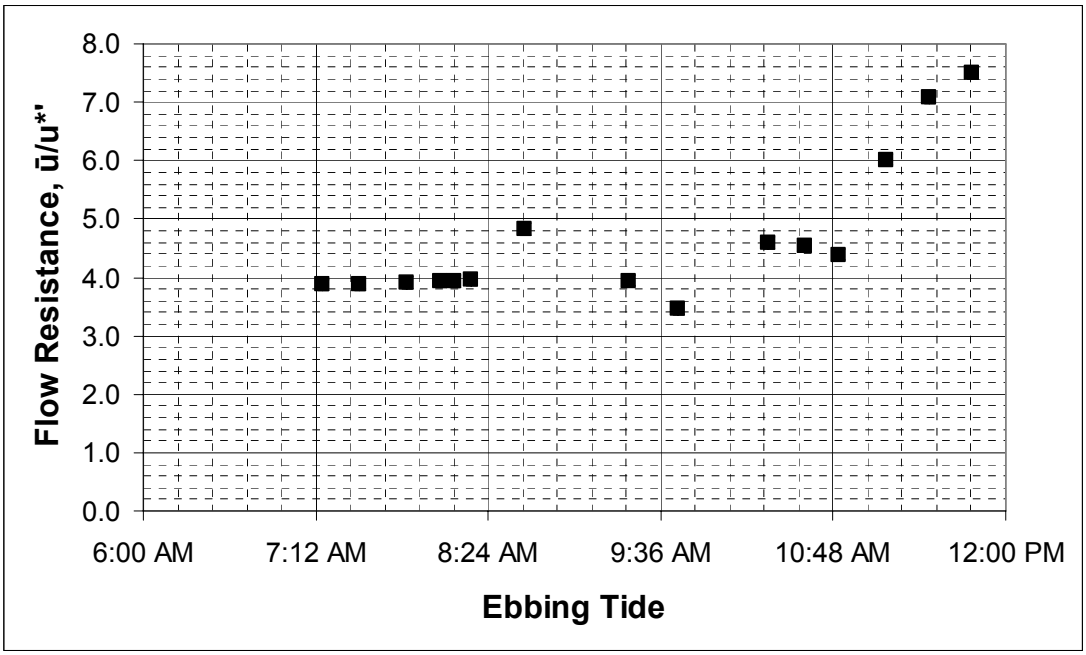

Figure 17: Flow resistance over time for site 1. Flow resistance is dimensionless and has a small range of values for this cross section. The error bars for these data are smaller than the data points; flow resistance has an error of ± 0.1 and time has an error of ± 1 minute.

Total flow resistance is highest near maximum discharge, which lags almost 2 hours behind maximum tidal height (note that velocity and thus discharge are zero at maximum tidal stage, which occurs before the tide changes). Manning's n decreases as the tide goes out (or in) due to the flattening of the vegetation (Figure 18c). This high flow resistance near maximum discharge is opposite of what would normally be expected for channels without vegetation that flattens with time. Note that the vegetation has to change the flattening direction during the tidal cycle, which also contributes to flow resistance at high tides.

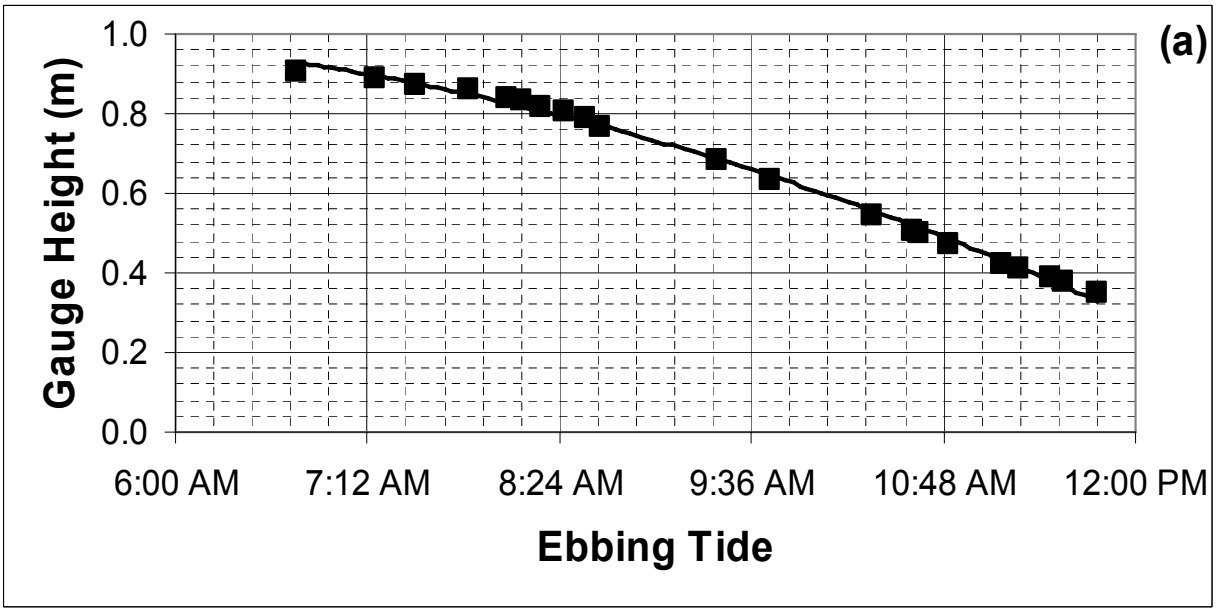

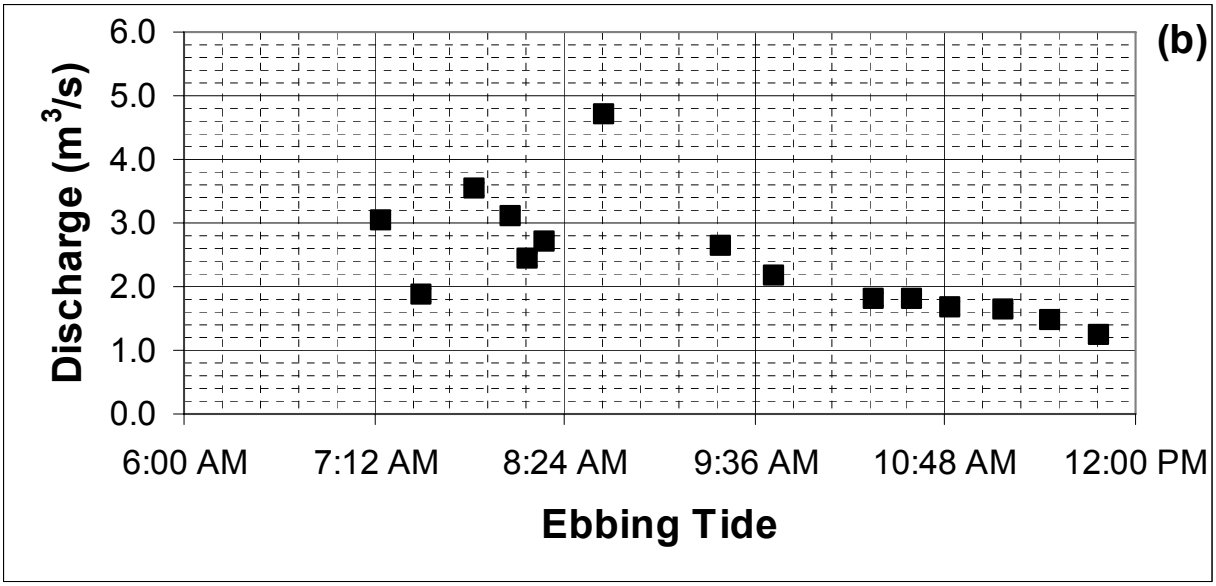

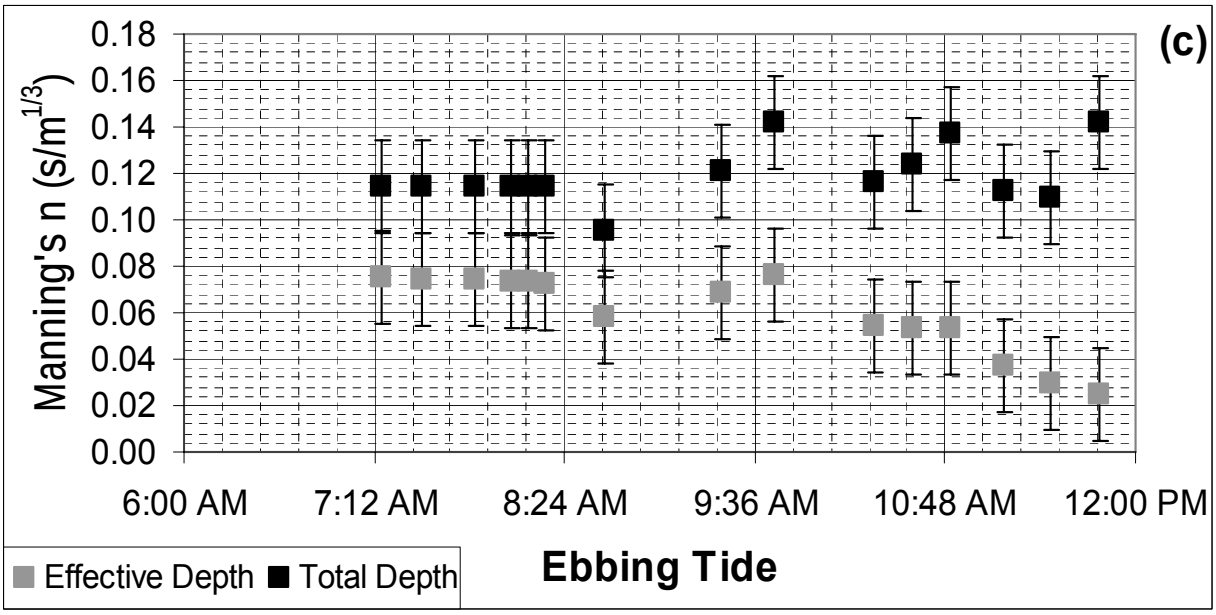

Figure 18a-c: These series of graphs show the trend in gauge height decline, the timing of peak discharge and Manning's n values as a function of time. (a) Gauge height as a function of time at site 1. The error bars for these data are smaller than the data points. (b) Discharge as a function of time at site 1 during ebbing tide. The error bars for these data are smaller than the data points; the error bars for discharge are $\sigma_Q = \pm 0.1$ m^3/s due to depth, width and mean velocity errors. (c) Manning's n has been calculated using the total depth (H) where $n = (H^{0.67}S^{0.50})/\bar{u}$. Manning's n has also been calculated using effective depth (H – Zm) where $n' = ((H - Zm)^{0.67}S^{0.50})/\bar{u}$. The error bars for both Manning's values represent ± 0.02 $s/m^{1/3}$ error due to depth, gradient and mean velocity errors; the error bars for time are smaller than the data points.

Visual observations of the vegetation during the tidal cycle agree with flow resistance values presented in Figures 17 and 18c. As the tide begins to fall, the vegetative canopy is upright, but waves in the water. As the water level continues to drop, the velocity increases and the vegetation begins to deflect downstream. This flattening of the vegetation in the direction of flow creates a smoothing of the channel and further increases the flow velocities.

As previously discussed, Lawrence et al. (2004) used a hydrodynamic model to determine the effects of Manning's roughness values on peak discharge in tidal flow. They used three different values of Manning's n (0.07, 0.15 and 0.50). Under vegetated conditions, taking into account the effective depth, Manning's n peaks at 0.076 $m^{-1/3}s$, indicating that Manning's roughness values of greater than 0.50 are highly unlikely and should not be used for tidal flow modeling. In most studies, however, the effective depth is not known, so Manning's n values of the total channel are used. In this study of the Patuxent Tidal channels, use of total depth rather than effective depth indicates a maximum Manning's n value of 0.14 $m^{-1/3}s$, which is similar to Lawrence's central estimate. Most importantly, as can be seen in Figure 18c, Manning's roughness coefficients do not remain constant as typically assumed in hydrodynamic models.

4.4 Effect of flow resistance on travel distances into the marsh

Extensive vegetation on channel beds can affect the conveyance area in the channel, the flow resistance in the channel, flow velocities, and shear velocities. In the previous sections, I presented data on the effects of *Hydrilla* growth on velocity, flow resistance, and the hydraulic geometry characteristics of tidal channels. In this section, I will use the field measurements of velocity to evaluate the distances that parcels of water could travel during incoming tides. In the next section, I will evaluate the consequences of the channel hydraulics on sediment transport in the channels.

For the calculation of travel times and therefore travel distances, I will use field values of channel velocities measured at the mouth of the tidal network (site 1). This site had the highest velocities; therefore, the resulting calculations should provide estimates for the maximum distances that parcels of water could travel with extensive *Hydrilla* growth on the channel beds. Calculations were made for the duration of a tidal half-period and travel distances were determined for a wide variety of tidal conditions (Figure 19). Determining the travel distances for water from the network mouth upstream through the system constrains the maximum distance that sediment can travel under various velocities and tidal half-period lengths.

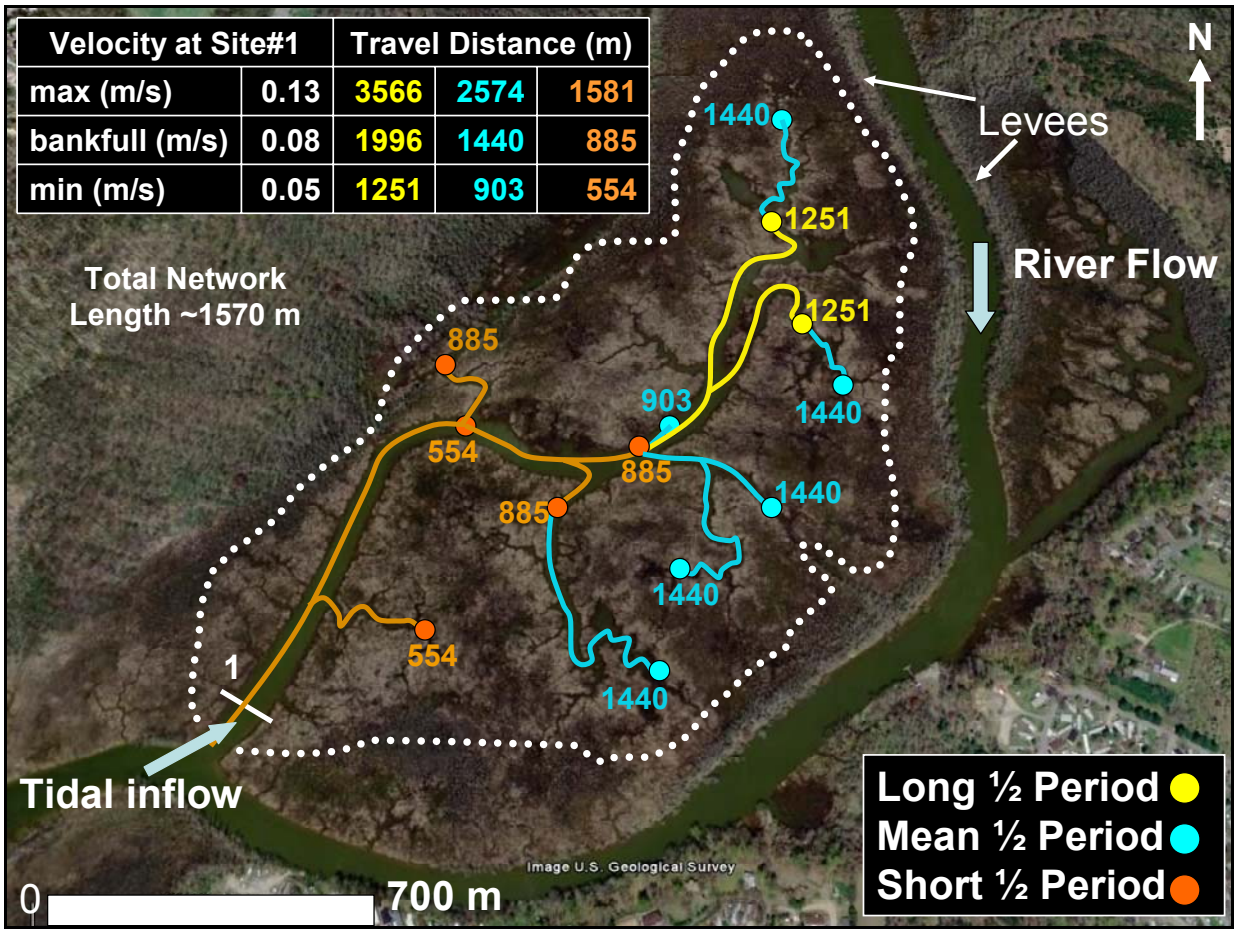

Figure 19: Travel distances for water moving from the network mouth up through the tidal system under various conditions including velocity and tidal half-period. Three channel velocities were used (maximum, average and minimum) along with three tidal half-periods (long, average and short) to find the travel distance. A tidal half-period begins at high tide and ends at the following low tide. (March 2007 image by US Geological Survey accessed through Google Earth).

The channel velocities were measured in field conditions for the expected high tide in a lunar month. In addition to tidal stage variations, tidal period also varies. During the longest tidal half-period, the velocity must be greater than the minimum velocity observed in order for water to be transported from the mouth to the upper-most reaches of the network. During the average tidal half-period, the channel velocity must be greater than the average velocity and during the shortest tidal half-period, the channel velocity must be significantly greater than the average velocity in order for water to reach the upper-most reaches of the network. For the average tidal half-period, water will not reach the upper-most reaches of the network. Thus, organic matter and sediment that the water is carrying will also not reach the upper portions of the marsh network.

To estimate the bankfull channel velocity during non-vegetated conditions the Manning equation is invoked. This requires two assumptions: the first assumption is that Manning's n is equal to the typical roughness value for terrestrial streams (n = 0.035) and the second assumption is that gradient remains constant from vegetated to non-vegetated conditions so that the gradient measured at bankfull during vegetative maxima can be used for vegetative minima. The Manning's n values determined for this section of the network, during vegetative maxima range

from 0.025 to 0.037 $m^{-1/3}s$. This range could be lower than the non-vegetative channel bed roughness due to the flattening and smoothing of the vegetation. Thus, assuming a Manning's n value at the upper bound of the lower range seems practical and well supported.

Table IV: Water Travel Distances

Tidal Half-Period (hours)			Long	Mean	Short
			7.39	5.34	3.28
Velocity at Site 1 (m/s)			Travel Distance (m)		
Max SAV	Maximum	0.13	3566	2574	1581
	Bankfull	0.08	1996	**1440**	**885**
	Minimum	0.05	**1251**	**903**	**554**
Min SAV	Bankfull	0.23	6224	4492	2759
Travel distances in red are less than the total network length (~1570 m)					

4.5 Maximum shear velocity and suspended sediment transport

Flow hydraulics can have several consequences for wetland maintenance. Organic debris and sediment can be brought into channels and deposited on marsh surfaces during high tides. The accumulation of organic matter and sediment can be additional components of the accumulation budget in addition to *in situ* organic matter accumulation (Morris et al., 2002). Organic matter can be carried into the marshes with overbank flows, provided that water is carried into the marshes (Rybczyk and Cahoon, 2002). Sediment, however, can be dropped out of the flow during the tidal cycle. The ability of a flow to transport sediment can be evaluated with the ratio of the fall velocity of the sediment (constrained by grain size and shape) and the shear velocity of the fluid. As described previously, shear velocity is calculated from the energy gradient, flow depth, and gravitational acceleration. The height of the SAV remains constant and/or increases upstream. Channel depth decreases upstream therefore decreasing the effective cross sectional area and thus decreasing shear velocity as indicated in Figure 20.

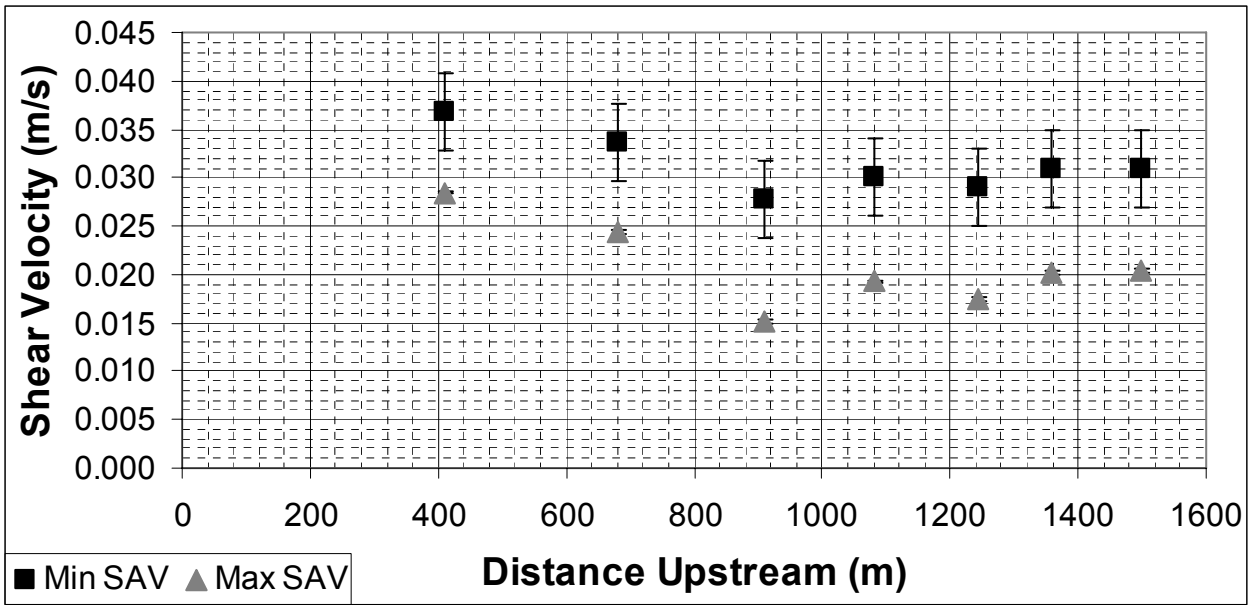

Figure 20: Shear velocity as a function of distance from the network mouth. Shear velocity is calculated assuming constant energy gradient and vegetative height. The error bars show ± 0.004 m/s error with respect to minimum SAV shear velocity and ± 0.0002 m/s error with respect to maximum SAV shear velocity; the error bars for distance upstream are smaller than the data points.

Using the shear velocity in the downstream region and the Rouse equation for various sediment sizes, overbank deposits in this downstream region will consist of only clay and silt, during maximum SAV growth. In the upstream regions, overbank deposits will comprise clay and silt, with a greater proportion of clay than the downstream. During periods of minimum SAV, downstream overbank deposits will consist of clay, silt, *very* fined-grained sand and a small fraction (< 10%) of fine-grained sand. Similarly, upstream overbank deposits during non-vegetated conditions consist of clay, silt and a small fraction (< 20%) of *very* fine-grained sand. These estimates are considered rough, as they are based on a constant energy gradient and constant vegetative height throughout the network. While these are rough estimates, they are verified by field observations of bank slope. Low sloped banks indicate larger grain sizes, whereas vertical banks indicate smaller, clay-like grain sizes. This network contains low slopes in the downstream regions and greater to nearly vertical bank slopes in the upstream regions, which demonstrates a decrease in grain size deposition upstream.

Conclusions and Discussion

Tidal channels are designed by nature to effectively convey water and sediment into marsh interiors. Flow velocities are maintained for bankfull flows by width restriction in the upstream direction (Langbein, 1963; Pillsbury, 1953). Therefore, the downstream hydraulic geometry for tidal channels should show significant exponents for width, but an almost constant velocity, and therefore low exponents for velocity. A constant velocity is not seen in the *Hydrilla* dominated channels. In fact, the channels show a rapid upstream decrease in velocity and thus discharge carried by the channels.

Flow resistance coefficients are very high in comparison to average terrestrial streams. Manning's n values are much higher than for terrestrial channels. Average Manning's n for a

similar terrestrial channel is approximately 0.035 $m^{-1/3}s$, similar to what these channels exhibited with flattening of the vegetation. High flow resistance values for high flow significantly reduces the discharge that can move into the tidal channels. Hydraulic roughness (Manning's n) for the bankfull and other stages increases upstream, which gives lower velocities for similar depths. A reduction in discharge is also seen in the downstream hydraulic geometry. Discharge during vegetative maxima is almost an entire order of magnitude smaller than discharge during vegetative minima. This decrease in discharge with increasing vegetation is demonstrated visually by a shift in the downstream plots and numerically by a shift in the coefficients.

The at-a-station hydraulic geometry exponents demonstrate spatial differences in *Hydrilla* growth. Channels in different parts of the system have different at-a-station characteristics. Velocity exponents decrease in the upstream direction indicating that some hydraulic force is causing velocity to accommodate the changing discharge. The proportion of SAV in the channel area also increases upstream and as the tide drains in the upper reaches the top of the vegetative canopy sits at water level leading to the drastic decrease in velocity as represented in the larger values of *m* for the upstream sites. Plotting each cross section on the b-f-m ternary diagram shows that at least one of the upstream channels is becoming unstable during maximum vegetation. The same channel that lies outside the boundary outlines on the b-f-m ternary diagram (site 6) also lies outside of the increasing trend in shape factor in the upstream direction.

In terrestrial settings, the shape factor tends to increase in the downstream direction, transitioning from deep, narrow channels upstream to shallow, wide channels downstream. This phenomenon is due to the decrease in gradient downstream and therefore an increasingly wider floodplain available to accommodate wider, shallower channels. In this system and in other tidal networks the opposite effect occurs because the tide must form the channel from downstream to upstream. Therefore, the downstream reaches are formed first and most often, resulting in the exponential decrease in width upstream, describe by Pillsbury (1956) and later revisited by Langbein (1963). The coupled decrease in depth upstream at a slower rate than width maintains the increasing shape factor. When additional flow resistance is introduced into a channel, it must accommodate for this via changes in velocity, gradient and/or depth.

The presence of vegetation lowers the effective cross sectional area, which affects discharge. The proportion of SAV in a cross section increases upstream; this affects the at-a-station and downstream hydraulic geometry. Due to this decrease in the carrying capacity of the channels, overbank flooding occurs disproportionately in the lower reaches of the marsh; this maintains the lower marsh through deposition of sediment. The lower portions of the Patuxent marsh studied in this report shows significant reaches of "high" marsh with shrub rather than wetland vegetation that might be caused by this process.

Mean channel velocities limit transport distances of water and sediment into the marsh. Transport distances are less than the total channel length during vegetated conditions. With *Hydrilla* present, shear velocities can only convey silt and clay into the mouth and only clay into upper marsh reaches. Under non-vegetated conditions, shear velocities can transport a small fraction of sand into the mouth. Therefore, the lack of upstream sediment deposition will make it difficult for the upper reaches of the network to keep pace with sea level rise. This deterioration has been observed in interior tidal network marshes across the globe (Kirwan and Murray, 2007; Rinaldo et al., 2004; Rybczyk and Cahoon, 2002).

Modeling the effect of long-term sea level rise is very important for evaluation of potential impacts on coastal ecosystems and cities. Field data on vegetation heights, vegetative

flow resistance, and other data from studies similar to this one could greatly improve modeling of flow and sediment in tidal systems. Typically, cross sectional area and velocity parameters are input to the model, but this does not factor in the flow resistance or non-flow-area that vegetation creates. This study demonstrates that SAV has a significant effect on the mean channel velocity, discharge, and shear velocity of a tidal network. The consequence of a reduction in these hydraulic variables is a reduction in both water and sediment fluxes into the channels and thus marsh maintenance, especially in the upper reaches. Most importantly, this study demonstrates the need for a variable or seasonal flow resistance parameter in hydrodynamic modeling of tidal marsh systems with SAV.

References

Bradshaw, P., and Huang, G.P., 1995, The law of the wall in turbulent flow: Proceedings: Mathematical and Physical Sciences, v. 451, p. 165-188.

Buchanan, T.J., and Somers, W.P., 1969, Techniques of Water-Resources Investigations of the United States Geological Survey, Book 3, Chapter A8, 65 p.

Carollo, F.G., Ferro, V., and Termini, D., 2002, Flow velocity measurements in vegetated channels: Journal of Hydraulic Engineering, v. 128, p. 664-673.

Chen, Yen-Chang and Chiu, Chao-Lin, 2002, An efficient method of discharge measurement in tidal streams: Journal of Hydrology, v. 265, p. 212-224.

Dingman, S.L., 2007, Analytical derivation of at-a-station hydraulic-geometry relations: Journal of Hydrology, v. 334, p. 17-27.

Hershner, C., and Havens, K.J., 2008, Managing invasive aquatic plants in a changing system: Strategic consideration of ecosystem services: Conservation Biology, v. 22, p. 544-550.

Hicks, S.D., 2006, Understanding Tides, Center for Operational Oceanographic Products and Services, U.S. Department of Commerce, National Oceanic and Atmospheric Administration, 76 p.

Hughes, C.E., Binning, P., and Willgoose, G.R., 1998, Characterisation of the hydrology of an estuarine wetland: Journal of Hydrology, v. 211, p. 34-49.

Kirwan, M.L. and Murray, A.B., 2007, A coupled geomorphic and ecological model of tidal marsh evolution: Proceedings of the National Academy of Sciences of the Unites States of America, v. 104, p. 6118-6122.

Kosiba, A.J., 2008, Stability of gravel bars and bedload transport in Paint Branch Creek: University of Maryland Geology Senior Thesis, College Park, MD, 45 p.

Langbein, W.B., 1963, The hydraulic geometry of a shallow estuary. Bulletin of the International Association of Scientific Hydrology, v. 8, p. 84-94.

Lawrence, D.S.L., Allen, J.R.L., and Havelock, G.M., 2004, Salt marsh morphodynamics: An investigation of tidal flows and marsh channel equilibrium: Journal of Coastal Research, v. 20, p. 301-316.

Leopold, L.B. and Maddock, Jr., T., 1953, The Hydraulic Geometry of Stream Channels and Some Physiographic Implications, U.S. Geological Survey Professional Paper 252, 56 p.

Morris, J.T, Sundareshwar, P.V., Nietch, C.T., Kjerfve, B., and Cahoo, D.R., 2002, Responses of coastal wetlands to rising sea level: Ecology, v. 83, p. 2869-2877.

Morse, J.L., Megonigal, J.P., and Walbridge, M.R., 2004, Sediment nutrient accumulation and nutrient availability in two tidal freshwater marshes along the Mattaponi River, Virginia, USA: Biogeochemistry, v. 69 p. 175-206.

Myrick, R.M. and Leopold, L.B., 1963, Hydraulic Geometry of a Small Tidal Estuary, U.S. Geological Survey Professional Paper 422-B, 18 p.

Nepf, H. and Ghisalberti, M., 2008, Flow and transport in channels with submerged vegetation: Acta Geophysica, v. 56, p. 753-777.

Nyman, J.A. and DeLaune, R.D., 1999, Four potential impacts of global sea-level rise on coastal marsh stability: Current Topics in Wetland Biogeochemistry, v. 3, p. 112-117.

Orth, R.J., and Moore, K.A., 1984, Distribution and abundance of submerged aquatic vegetation in Chesapeake Bay: An historical perspective: Estuaries, v. 7, p. 531-540.

Prandtl, L., 1952, Essentials of fluid dynamics: New York, Hafner Publishing Company, 452 p.

Rhodes, D.D., 1977, The b-f-m diagram: Graphical representation and interpretation of at-a-station hydraulic geometry: American Journal of Science, v. 277, p. 73-96.

Rinaldo, A., Belluco, E., D'Alpaos, A., Feola, A., Lanzoni, S., and Marani, M., 2004, Tidal networks: Form and function: Coastal and Estuarine Sciences, v. 59, p. 75-91.

Rybczyk, J.M. and Cahoon, D.R., 2002, Estimating the potential for submergence for two wetlands in the Mississippi River Delta: Estuaries, v. 25, p. 985-998.

Rybicki, N.B. and Landwehr, J.M., 2007, Long-term changes in abundance and diversity of macrophyte and waterfowl populations in an estuary with exotic macrophytes and improving water quality: Limnology and Oceanography, v. 52 p. 1195-1207.

Tiner, R.W., 2005, Assessing cumulative loss of wetland functions in the Nanticoke River watershed using enhanced National Wetlands Inventory data: Wetlands, v. 25, p. 405-419.

Turner, R.E., Howes, B.L., Teal, J.M., Milan, C.S., Swenson, E.M., and Goehringer-Toner, D.D., 2009, Salt marshes and eutrophication: an unsustainable outcome: Limnology and Oceanography, v. 54, p. 1634-1642.

Wilson, C.A.M.E., 2007, Flow resistance models for flexible submerged vegetation: Journal of Hydrology, v. 342, p. 213-222

Wang, F.C., Lu, T., and Sikora, W.B., 1993, Intertidal marsh suspended sediment transport processes, Terrebonne Bay, Louisiana, U.S.A.: Journal of Coastal Research, v. 9, p. 209-220.

Wu, F.C., Shen, H.W., and Chou, Y.J., 1999, Variations of roughness coefficients for unsubmerged and submerged vegetation: Journal of Hydraulic Engineering, v. 125, p. 934-942.

Acknowledgements

First, I would like to thank my advisor, Dr. Karen Prestegaard, for her support, never-ending knowledge and encouragement. Through her mentorship, she has taught me many invaluable field techniques and has helped me strengthen my critical thinking skills. Throughout this process, she has been a source of motivation and encouragement.

I would also like to thank Emily Seldomridge for her help in and out of the field. Emily has also been a source of motivation; her excitement about my project has encouraged me to focus and work hard.

A special thanks goes to my ecology professor, Dr. Bob Ford, at Frederick Community College for introducing me to the beauty of freshwater wetlands. During a field trip to Jug Bay Wetland Sanctuary, the balance between ecological complexity and pure calmness exhibited by the waters enchanted me.

Finally, I would like to thank my family and my boyfriend, Brian. Without their unrelenting support and encouragement, I would not have challenged myself to get to this point. Since day one, they have believed in me, even when I have not believed in myself. They have taught me to work hard and always put forth my best effort.

Appendix A: Data Tables for Figures

Table A: Gauge height data from October 11, 2009, used in Figure 7.

Downstream: Site 4		Upstream: Site 5	
Time $\sigma_{time} = \pm$ 1 min	Gauge Height (m) $\sigma_{GH} = \pm$ 0.002 m	Time $\sigma_{time} = \pm$ 1 min	Gauge Height (m) $\sigma_{GH} = \pm$ 0.002 m
12:20 PM	0.597	12:30 PM	0.756
12:32 PM	0.579	12:43 PM	0.732
12:46 PM	0.561	12:50 PM	0.722
12:52 PM	0.549	12:55 PM	0.713
12:57 PM	0.539	1:00 PM	0.707
1:02 PM	0.530	1:05 PM	0.695
1:07 PM	0.521	1:10 PM	0.686
1:12 PM	0.512	1:15 PM	0.677
1:17 PM	0.503	1:20 PM	0.668
1:22 PM	0.494	1:25 PM	0.658
1:27 PM	0.485	1:30 PM	0.649
1:32 PM	0.475	1:35 PM	0.640
1:37 PM	0.463	1:40 PM	0.628
1:42 PM	0.454	1:45 PM	0.619
1:47 PM	0.445	1:50 PM	0.607
1:52 PM	0.433	1:55 PM	0.597
1:57 PM	0.424	2:00 PM	0.585
2:02 PM	0.411	2:05 PM	0.576
2:07 PM	0.399	2:10 PM	0.561
2:12 PM	0.387	2:15 PM	0.552
2:17 PM	0.378	2:20 PM	0.543
2:22 PM	0.366	2:25 PM	0.530
2:27 PM	0.354	2:30 PM	0.515
2:32 PM	0.341	2:35 PM	0.506
2:37 PM	0.332	2:40 PM	0.494
2:42 PM	0.320	2:45 PM	0.482
2:47 PM	0.308	2:50 PM	0.469
2:52 PM	0.296	2:55 PM	0.457
2:57 PM	0.283	3:00 PM	0.445
3:02 PM	0.271	3:05 PM	0.433
3:07 PM	0.262	3:10 PM	0.421
3:12 PM	0.250	3:15 PM	0.408
3:17 PM	0.235	3:20 PM	0.396
		3:54 PM	0.323

Table B: Gauge height and cross sectional area data for site 1, collected July 7, 2009, used in Figure 10.

Site 1	
Gauge Height (m) $\sigma_{GH} = \pm 0.002$ m	Cross Sectional Area (m^2) $\sigma_A = \pm 1.14$ m^2
0.457	41.11
0.408	39.08
0.320	35.41
0.280	33.77
0.244	32.28
0.198	30.47
0.165	29.2
0.122	27.59

Table C: At-a-station hydraulic geometry for site 2, data collected July 7, 2009, used in Figures 12a-c. The power equations for this cross section are $w = 17.4Q^{0.20}$, $d = 0.50Q^{0.32}$ and $\bar{u} = 0.12Q^{0.48}$. Using the continuity of discharge we can check that the power equations are valid so long as the exponents and coefficients sum and multiply, respectively to unity: $0.20 + 0.32 + 0.48 = 1.00$ and $17.4 \cdot 0.50 \cdot 0.12 = 1.0$.

Site 2			
Width (m) $\sigma_w = \pm 0.1$ m	Depth (m) $\sigma_d = \pm 0.04$ m	Velocity (m/s) $\sigma_{\bar{u}} = \pm 0.01$ m/s	Discharge (m^3/s) $\sigma_Q = \pm 0.1$ m^3/s
18.0	0.55	0.11	1.1
17.5	0.49	0.11	0.9
16.5	0.48	0.09	0.7
15.5	0.44	0.10	0.7
14.5	0.40	0.09	0.5
14.5	0.36	0.06	0.3
13.5	0.34	0.08	0.4
13.5	0.29	0.09	0.4
12.0	0.30	0.04	0.1

Table D: At-a-station hydraulic geometry for site 1, data collected July 7, 2009, used in Figure 13a. The power equations for this cross section are $w = 30.1Q^{0.27}$, $d = 0.66Q^{0.27}$, and $\bar{u} = 0.050Q^{0.46}$. Using the continuity of discharge we can check that the power equations are valid so long as the exponents and coefficients, sum and multiply, respectively to unity: 0.27 + 0.27 + 0.46 = 1.00 and 30.1 · 0.66 · 0.05 = 1.0.

Site 1			
Width (m) $\sigma_w = \pm$ 0.1 m	Depth (m) $\sigma_d = \pm$ 0.04 m	Velocity (m/s) $\sigma_{\bar{u}} = \pm$ 0.01 m/s	Discharge (m^3/s) $\sigma_Q = \pm$ 0.1 m^3/s
41.0	0.98	0.08	3.0
41.0	0.97	0.05	1.9
41.0	0.95	0.09	3.5
41.0	0.93	0.08	3.1
41.0	0.93	0.06	2.4
40.9	0.91	0.07	2.7
40.9	0.86	0.13	4.7
40.1	0.79	0.08	2.6
39.6	0.76	0.07	2.2
37.0	0.72	0.07	1.8
33.0	0.77	0.07	1.8
32.8	0.74	0.07	1.7
31.9	0.71	0.07	1.6
31.7	0.68	0.07	1.5
30.0	0.68	0.06	1.2

Table E: At-a-station hydraulic geometry for site 3, data collected July 7, 2009, used in Figure 13b. The power equations for this cross section are $w = 15.0Q^{0.04}$, $d = 0.54Q^{0.56}$, and $\bar{u} = 0.12Q^{0.40}$. Using the continuity of discharge we can check that the power equations are valid so long as the exponents and coefficients, sum and multiply, respectively to unity: 0.04 + 0.56 + 0.40 = 1.00 and 15.0 · 0.54 · 0.12 = 1.0.

Site 3			
Width (m) $\sigma_w = \pm$ 0.04 m	Depth (m) $\sigma_d = \pm$ 0.04 m	Velocity (m/s) $\sigma_{\bar{u}} = \pm$ 0.01m/s	Discharge (m^3/s) $\sigma_Q = \pm$ 0.1 m^3/s
15.7	1.14	0.16	3.0
15.2	0.69	0.17	1.8
15.2	0.69	0.14	1.5
15.2	0.66	0.15	1.5
15.2	0.61	0.18	1.7
15.2	0.60	0.14	1.3
15.2	0.59	0.14	1.2
15.2	0.54	0.13	1.0
14.9	0.50	0.11	0.8
14.9	0.49	0.12	0.9
14.9	0.46	0.10	0.7

Table F: At-a-station hydraulic geometry for site 6, data collected August 7, 2009, used in Figure 13c. The power equations for this cross section are $w = 10.6Q^{0.01}$, $d = 0.44Q^{0.02}$, and $\bar{u} = 0.21Q^{0.97}$. Using the continuity of discharge we can check that the power equations are valid so long as the exponents and coefficients, sum and multiply, respectively to unity: 0.01 + 0.02 + 0.97 = 1.00 and 10.6 · 0.44 · 0.21 = 1.0.

Site 6			
Width (m) $\sigma_w = \pm$ 0.04 m	Depth (m) $\sigma_d = \pm$ 0.04 m	Velocity (m/s) $\sigma_{\bar{u}} = \pm$ 0.01m/s	Discharge (m^3/s) $\sigma_Q = \pm$ 0.1 m^3/s
10.4	0.71	0.01	0.1
10.4	0.69	0.01	0.1
10.4	0.67	0.00	0.0
10.4	0.64	0.00	0.0
10.4	0.59	0.00	0.0
10.4	0.53	0.01	0.1
10.4	0.52	0.01	0.1
10.4	0.47	0.02	0.1
10.4	0.43	0.04	0.2
10.4	0.41	0.02	0.1
10.4	0.39	0.02	0.1
10.2	0.37	0.00	0.0
10.2	0.35	0.02	0.1
10.2	0.32	0.03	0.1

Table G: At-a-station hydraulic exponents and coefficients for site 1, 2, 3, 6 and 7 as a function of distance upstream from the network mouth, used in Figures 15a-c. This table is also located within the text on page 19.

Site #	1	2	3	6	7
Distance upstream (m)	59	236	557	1097	1097
Exponent b (width)	0.27	0.20	0.04	0.01	0.01
Exponent f (depth)	0.27	0.32	0.56	0.02	0.29
Exponent m (velocity)	0.46	0.48	0.40	0.97	0.70
Coefficient a (width)	30.1	17.4	15.0	10.6	6.6
Coefficient c (depth)	0.66	0.50	0.54	0.44	0.51
Coefficient k (velocity)	0.050	0.12	0.12	0.21	0.30
Shape factor (f/b)	1.0	1.6	14	2.0	29
b + f + m	1.00	1.00	1.00	1.00	1.00
a*c*k	1.0	1.0	1.0	1.0	1.0

Table H: Maximum channel depth and downstream hydraulic geometry during maximum SAV and minimum SAV, used in Figure 16a-c. For reference against average channel depth, the maximum channel depth is presented with the downstream hydraulic geometry. The power equations that relate width, depth and velocity to discharge for the main channel during maximum vegetation are $w = 17.9Q^{0.70}$; $d = 0.92Q^{0.07}$; $\bar{u} = 0.061Q^{0.23}$. Using the continuity of discharge we can check that the power equations are valid so long as the exponents and coefficients, sum and multiply, respectively to unity: $0.70 + 0.07 + 0.23 = 1.00$ and similarly, $17.9 \cdot 0.92 \cdot 0.061 = 1.0$. The power equations that relate width, depth and velocity to discharge for the main channel during minimum vegetation are $w = 6.2Q^{0.83}$; $d = 0.80Q^{0.10}$; $\bar{u} = 0.20Q^{0.07}$. Using the continuity of discharge we can check that the power equations are valid so long as the exponents and coefficients, sum and multiply, respectively to unity: $0.83 + 0.10 + 0.07 = 1.00$ and similarly, $6.2 \cdot 0.80 \cdot 0.20 = 1.0$.

Maximum Submerged Aquatic Vegetation				Maximum Channel Depth (m) $\sigma_d = \pm$ 0.04 m	Minimum Submerged Aquatic Vegetation			
Width (m) $\sigma_w = \pm$ 0.04 m	Depth (m) $\sigma_d = \pm$ 0.04 m	Velocity (m/s) $\sigma_{\bar{u}} = \pm$ 0.01m/s	Discharge (m^3/s) $\sigma_Q = \pm$ 0.1 m^3/s		Width (m) $\sigma_w = \pm$ 0.04 m	Depth (m) $\sigma_d = \pm$ 0.04 m	Velocity (m/s) $\sigma_{\bar{u}} = \pm$ 0.01m/s	Discharge (m^3/s) $\sigma_Q = \pm$ 0.1 m^3/s
3.4	0.89	0.04	0.1	1.10	3.4	0.89	0.22	0.7
9.4	0.88	0.05	0.4	1.17	9.4	0.88	0.21	1.8
12.5	0.78	0.05	0.5	1.03	12.5	0.78	0.20	1.9
16.9	0.84	0.06	0.8	1.23	16.9	0.84	0.21	3.0
31.5	0.71	0.07	1.5	1.11	31.5	0.71	0.19	4.2
30.5	1.05	0.07	2.4	1.82	30.5	1.05	0.24	7.8
30.5	1.25	0.08	3.0	2.06	30.5	1.25	0.27	10.4
41.7	0.99	0.08	3.3	2.01	41.7	0.99	0.23	9.5

Table I: Time series of roughness, gauge height, and discharge at the network mouth, data collect July 7, 2009, used in Figure 17 and 18a-c.

Time $\sigma_{time} = \pm 1$ min	Flow Resistance ($\bar{u}/u^{*\prime}$) $\sigma_{\bar{u}/u^{*\prime}} = \pm 0.1$	Gauge Height (m) $\sigma_{GH} = \pm 0.002$ m	Discharge (m^3/s) $\sigma_Q = \pm 0.1$ m^3/s	Manning's n ($s/m^{1/3}$) $\sigma_n = \pm 0.02$ $s/m^{1/3}$	Manning's n' ($s/m^{1/3}$) $\sigma_{n'} = \pm 0.02$ $s/m^{1/3}$
6:45 AM	0.0	0.908	0.0	0.00	0.00
7:15 AM	3.9	0.887	3.0	0.11	0.08
7:30 AM	3.9	0.875	1.9	0.11	0.07
7:50 AM	3.9	0.860	3.5	0.11	0.07
8:04 AM	3.9	0.838	3.1	0.11	0.07
8:10 AM	3.9	0.835	2.4	0.11	0.07
8:17 AM	3.9	0.817	2.7	0.11	0.07
8:39 AM	4.8	0.765	4.7	0.09	0.06
9:23 AM	3.9	0.683	2.6	0.12	0.07
9:43 AM	3.5	0.634	2.2	0.14	0.08
10:21 AM	4.6	0.546	1.8	0.12	0.05
10:36 AM	4.5	0.506	1.8	0.12	0.05
10:50 AM	4.4	0.470	1.7	0.14	0.05
11:10 AM	6.0	0.424	1.6	0.11	0.04
11:28 AM	7.1	0.390	1.5	0.11	0.03
11:46 AM	7.5	0.348	1.2	0.14	0.02

Table J: Maximum vegetative shear velocity (u*') and minimum vegetative shear velocity (u*) as a function of distance from the network mouth, used in Figure 20.

Distance Upstream from Mouth (m) $\sigma_{Dist} = \pm 1$ m	Total Depth Shear Velocity, u* (m/s) $\sigma_{u^*} = \pm 0.004$ m/s	Effective Depth Shear Velocity, u*' (m/s) $\sigma_{u^{*\prime}} = \pm 0.0002$ m/s
1498	0.031	0.0204
1359	0.031	0.0203
1244	0.029	0.0174
1081	0.030	0.0192
911	0.028	0.0152
680	0.034	0.0244
411	0.037	0.0285
59	0.033	0.0229

Appendix B: Honor pledge

I pledge on my honor that I have not given or received any unauthorized assistance or plagiarized on this assignment.

_____

Brittany Jenner